Modulating Soft Matter Friction Using Opposable Ultrasonic Vibrations

Didi van Dijk

Modulating Soft Matter Friction Using Opposable Ultrasonic Vibrations

by

D. van Dijk

to obtain the degree of Master of Science

at the Delft University of Technology,

to be defended on September 22nd 2022.

Acknowledgements

Modulating Soft Matter Friction Using Opposable Ultrasonic Vibrations

Didi van Dijk

Abstract—When we manipulate objects in our day-to-day life, we perceive information on the object via force feedback that we sense with our sensorimotor system. However, in virtual reality, we lack these forces, which makes it more challenging to interact with the digital world. Wearables, such as hand exoskeletons, can provide force feedback in VR. Nonetheless, as the devices' actuation or brake system is often bulky or heavy, users typically do not enjoy wearing them. In this study, we investigate the potential of a new friction-based mechanism that can address the existing issues. Our design adopts ultrasonic vibrations to generate a squeeze film, which is a well-studied phenomenon to decrease friction significantly. In literature, the phenomenon has only been investigated with vibrations from one side, with the goal of friction reduction. However, we show that by adding a vibrating surface opposite to the original one, we can extend the possibilities of squeeze films, enabling us to both decrease and increase friction. Since ultrasonic transducers can be miniaturized, our mechanism brings us closer to solving the size and weight issues of existing devices.

Index Terms—ultrasonic friction modulation, squeeze film, blocking mechanism, haptic feedback, wearables

✦

1 INTRODUCTION

In our search for the most delicious avocado in the supermarket, we do not only use our vision to inspect how ripe a fruit is but also our sense of touch to feel its softness and structure. We perceive the structure of an object by the resisting forces that are sensed by mechanoreceptors in our skin, joints, and muscles. The importance of these organs, and force feedback in general, is nicely illustrated in a video about a study by Johansson et al. [1], where they ask participants to light a match under two different conditions. During the first condition, participants have full sensory awareness of their hands. In the second condition, their fingers are injected with local anaesthesia, so no force feedback can be perceived. Without anaesthesia, participants light the match without any problems. However, with anaesthesia, we notice how participants become more clumsy, dropping the match multiple times, and requiring much more time to achieve their goal. This experiment is a classic example of how much we rely on force feedback and our sense of touch when interacting with the world around us.

Luckily, most of us can perceive these forces when interacting with objects in our day-to-day life. Nonetheless, we can now understand the challenges that arise when we shift from manipulating objects in the real world to manipulating them in the virtual world. Since virtual reality (VR) is currently rising in popularity for entertainment and training purposes to save time and costs, the demand for mechanisms that can provide force feedback in VR is increasing as well.

A way to provide this force feedback in VR is by utilizing wearable devices such as hand exoskeletons [3][4]. In hand exoskeletons, straps or linkages are attached to each finger that either move along with the fingers' movements, or statically stay in one position and block the fingers' movements. This blocking
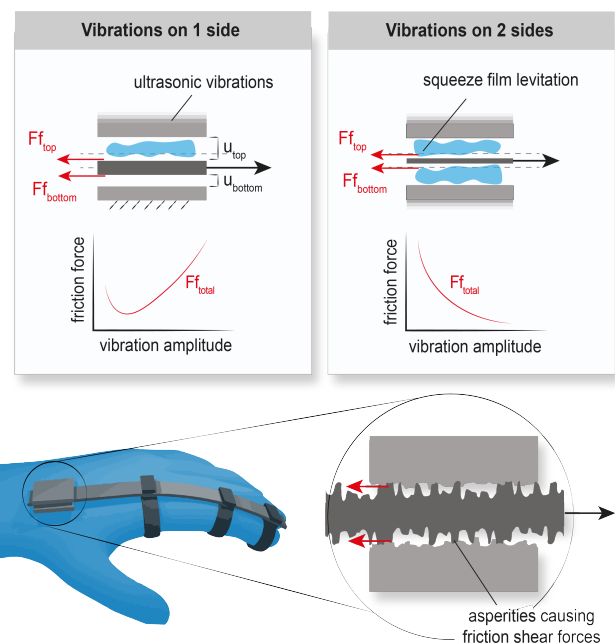
Fig. 1. Ultrasonic friction-based braking mechanism proposed in this study, and example of application derived from design [2]. $F_{f,top}$, $F_{f,bottom}$, and $F_{f,tot}$ are the friction force at the top, bottom, and in total, and u_{top} and u_{bottom} the interfacial separations.

action generates similar force feedback as to when interacting with an object without such a device. Traditionally, force feedback in hand exoskeletons is provided either via linkage systems [5], motor-tendon configurations [6], or pneumatic or fluidic bladders [7] which are attached to the fingers. Many of these state-of-the-art mechanisms can generate forces over $10N$, sufficient to manipulate objects in most daily-life activities [8]. However, because many devices are still tethered or rely on relatively bulky and heavy motors or pumps for their actuation, there are still issues when considering their wearability and portability [9].

Since the actuation or blocking mechanism is often the limiting factor for portable and lightweight designs [10], exploring other ways to block the finger's movements might solve the existing issues. For example, Hinchet et al. investigated the potential of electro-adhesion to block a finger motion [2]. Their design consisted of thin plates stacked on top of each finger which could slide over one another. However, when the plates were subjected to a voltage, electro adhesive forces made them stick together in the current position. No more motion could be achieved; thus, the fingers were blocked. With their original blocking mechanism, they succeeded in designing a lightweight exoskeleton, able to provide forces up to 20 N per finger. Nonetheless, they needed 1500 V to achieve this force, still requiring big and heavy power supplies. Therefore, their study also demonstrated that a mechanism based on electrostatics might not be the most promising solution. Even so, electrostatics is not the only technology by which we can modulate friction. Other friction-modulation mechanisms might still result in a small and lightweight design, while keeping it portable.

Another technique that is frequently used to modulate friction is adopting ultrasonic vibrations [11][12]. When applied at a high frequency ($> 20kHz$) and amplitude ($> 1\mu m$), ultrasonic vibrations can cause an effect better known as the squeeze film effect. In conventional designs, this thin, pressurized air film can levitate objects, leading to a significant reduction in friction. The technique has shown much potential in areas such as bearing technology [13][14] and haptic interfaces [15][16]. Therefore we want to investigate the potential of this technique for our application too.

State-of-the-art mechanisms adopt transducers that generate ultrasonic vibrations on one surface only. Matter that is placed on top of this surface can freely move vertically, levitating under the generated pressure. In our study, we add an extra constraint to this set-up: a second transducer placed on the other side of the matter lying on top of the original transducer. Due to this constraint, the material that is now clamped between two opposing transducers cannot levitate anymore but always stays in between the transducers. Nonetheless, if the middle layer consists of soft matter, it can change its thickness under compression and, therefore, also move up and down. Due to the soft matter's deformability, we expect that the addition of a second transducer enables us to either generate a squeeze film on one side of the middle layer or on both sides, as visualized in Fig. 1.

In this study, we demonstrate that a design with opposing transducers extends the possibilities of squeeze films, as opposing transducers can facilitate both a decrease and increase in friction (see Fig. 1). When both transducers are actuated, a squeeze film arising on both sides, significantly reduces friction.

On the other hand, when only one transducer is actuated, a squeeze film arising on this side decreases friction here, but at the same time the squeeze film pressure pushes the middle layer more closely to the opposite surface, increasing friction there. We show the increase in friction due to the pushing force of the squeeze film to be more significant than the decrease in friction at the transducer's side, leading to an increase in total friction. Both phenomena are interesting when designing a blocking mechanism for wearables: A friction-increase mechanism can provide active blocking, and a friction-decrease mechanism can allow for unrestricted movement and block a motion when turned off. Moreover, as ultrasonic transducers can be miniaturized, we believe that in the future, our mechanism can significantly reduce the size and weight issues of existing wearables.

2 BACKGROUND

2.1 Friction

Friction (F_f) is the force that resists the relative motion of two surfaces sliding against each other. On a macroscopic scale, it is calculated as $F_f = \mu F_N$, where F_N is the load force and μ the coefficient of friction. This coefficient is a non-dimensional scalar of which the value depends on both material properties, as well as on factors like sliding velocity and temperature.

On a microscopic scale, a critical factor influencing friction is surface roughness [17]. When zooming in on a surface, we find that it is never perfectly smooth but instead consists of a random height profile that can be approximated by a normal distribution (see Fig. 2) [18]. When two surfaces touch, the highest peaks of the opposite surfaces come into intimate contact and deform under the applied load force. The sum of all contact areas of the deformed asperities together is called the true area of contact. Each asperity in contact carries an adhesive shear load that is proportional to its contact area. All shear loads combined result in the total friction between the surfaces, which is thus linearly related to the true area of contact.
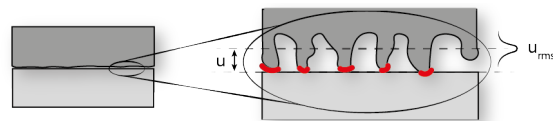
Fig. 2. Visualization of asperities, interfacial separation u and surface roughness u_{rms}. The sum of contact areas of individual asperities (in red) forms true area of contact.

The relationship for the true area of contact, thus also the total friction, can be derived from Persson's theory of contact [19]. This theory expresses the reaction force from the surfaces in contact as a function of the average gap between the surfaces u (also called the interfacial separation) and the surface roughness u_{rms}. Note that this surface roughness is the standard deviation of interfacial separation over

the lateral coordinates (SD $u(x, y)$). The reaction forces decrease over the interfacial separation by a negative exponential:

$$p_r = p_c exp \left(\frac{-u}{u_{rms}} \right). \qquad (1)$$

The variable p_c is the maximum absolute pressure given by $p_c = 0.375 q_0 u_{rms} E / (1 - v^2)$ [19]. Here, q_0 is the scale at which the u_{rms} is determined, E the Young's modulus, and v the Poisson ratio.

Via a derivation that takes into account the initial conditions at a given external load force (complete derivation in Appendix A), we find that the profile for the true area of contact also follows a negative exponential:

$$A = A_0 exp \left(\frac{-u + u_0}{u_{rms}} \right). \qquad (2)$$

In this formula, A is the calculated true area of contact, A_0 is the initial true area of contact, and u_0 is the initial interfacial separation. Since we have already concluded that the friction force is linearly related to this true area of contact, we can estimate it as:

$$F_f = F_{f,0} exp \left(\frac{-u + u_0}{u_{rms}} \right). \qquad (3)$$

Here, $F_{f,0}$ is the initial friction force corresponding to u_0. From equation 3 we can now appreciate that if we can control u, we can modulate friction.

2.2 Squeeze film theory

The interfacial separation u changes if the pressure of the fluid in the gap changes. As there can never be complete contact between surfaces, and instead, contact is formed by asperities, there is always some fluid present between the asperities (in case of a no vacuum environment). Now, if one of the opposing surfaces vibrates, and the surfaces move towards and away from each other, the fluid in between reacts. At low frequencies or gaps, the viscous forces in the fluid (often air) are relatively small, which means that the fluid is forced out of the gap when the surfaces move towards each other, and is sucked in when they move away from each other. However, when the vibration frequency is ultrasonic (typically >30 kHz), and the clearance is minimal (typically $< 10 \mu m$), the viscous forces increase and resist the fluid flow. Thus, the fluid becomes trapped between the surfaces [15]. The scenario with this trapped fluid is called the squeeze film effect, and can be compared to a piston inside a closed cylinder. Since the volume of the trapped fluid changes under compression, we know by Boyle's law ($pv = constant$) that the pressure changes too [20].

Salbu showed that the pressure and force profile of squeeze films are asymmetrical over the period of one oscillation [20]. Therefore, if the vibrations occur for a longer time, the time-averaged pressure of the
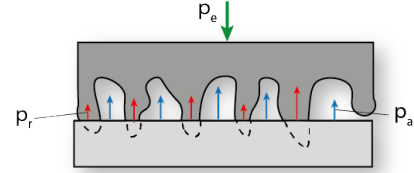
Fig. 3. Reaction force from support p_r, and squeeze film pressure p_a counterbalance load force p_e. Remake from [15].

fluid in the gap is higher than the initial pressure. If we recall the situation where we had one vibrating surface and an object on top of this vibrating surface, we can now imagine that the increase in pressure in between the surfaces, can levitate the object on top slightly above the vibrating surface. In this way, the interfacial separation increases so that fewer asperities are in intimate contact, and thus friction decreases.

Whether the fluid can be considered trapped can be tested by calculating the squeeze number σ. This number characterizes a non-dimensional ratio of the time required to squeeze out fluid from the gap, relative to the period of one oscillation. It is calculated as $\sigma = 12 \omega \mu L^2 / (p_0 u^2)$, with ω the angular frequency, μ the viscosity of the fluid, L the size of contact, and p_0 the ambient pressure. The higher the squeeze number, the lower the amount of fluid that dissipates at the edges of the contacting surfaces, thus the more the fluid can be considered trapped.

For the quantification of the amount of pressure that can be built up, various mathematical models have been employed. The most popular ones are based on the Rayleigh acoustic radiation pressure theory [21], and the Reynolds theory of gas film lubrication [20]. Zhao et al. showed that, depending on this squeeze number, certain models are more suited for the calculation of the pressure than others: for high squeeze numbers ($\sigma > 100$), the pressure can be best predicted using Reynolds equations, while for lower squeeze numbers, the acoustic radiation theory provides a better approximation [14]. In our experiment where $\omega \approx 250 \cdot 10^3$ rad/s, $\mu \approx 1.8 \cdot 10^{-5} kg/(ms)$ $L \approx 10^{-2}$ m, and $u \approx 10^{-5}$ m, we obtain a squeeze number of $\sigma \approx 500$. Therefore we approximate our pressure with the Reynolds theory, given by:

$$p_a = \frac{5}{4} p_0 \frac{\alpha^2}{u^2}. \qquad (4)$$

In this formula, α is the vibration amplitude.

2.3 Force balance

Now that we obtained a relationship for both the reaction forces from the support p_r and the squeeze film pressure p_a as a function of u, we need one more force to find a force balance by which we can calculate u itself. When two surfaces touch, p_r and p_a together counterbalance an external pressure p_e. This
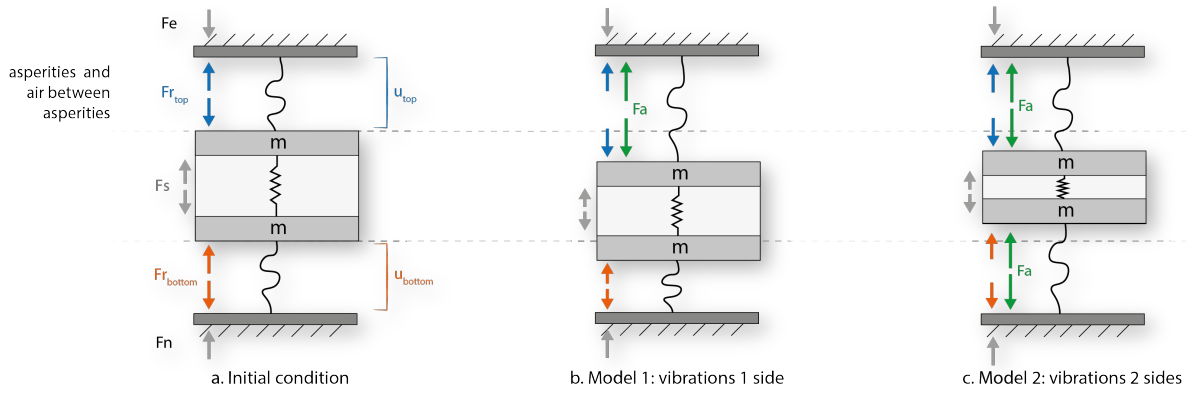
Fig. 4. **a.** Force balance initial condition, when no vibrations are yet applied. The interfacial separation at the top and bottom surface are given by u_{top} and u_{bottom}. The external force resulting from compression at the top is denoted F_e. The reaction force of the asperities in contact at the top and bottom are Fr_{top} and Fr_{bottom} respectively. As these reaction forces change non-linearly over the interfacial separation, we visualized it as a non-linear spring. The soft middle layer is modelled as two masses with a spring in between. The spring with spring force F_s accounts for the elastic behavior of the layer. **b.** Only top surface vibrates and causes a squeeze film force F_a there. **c.** Top and bottom surface are vibrating, so on both sides of the middle layer a squeeze film arises.

external pressure arises from the mass of an object on top or some initial compression. The force balance is visualized in Fig. 3 and is calculated as follows:

$$p_e = p_a + p_r, \tag{5}$$

and

$$p_e = \frac{5}{4} p_0 \frac{\alpha^2}{u^2} + p_c exp\left(\frac{-u}{u_{rms}}\right). \tag{6}$$

As p_e, p_0, α, u_{rms}, and p_c are generally known or can be measured or controlled, distance u can now be calculated. Moreover, since we already have an expression for the friction force that depends on u (see Eq. 3), we can now study the change in friction under the influence of a change in the variables mentioned earlier. Most studies express friction as a function of the vibration amplitude α [14][15][22], as this is often an accessible variable to control. Note that the initial variables that we mentioned before (A_0, $F_{f,0}$ and u_0) are variables in absence of vibrations, so for $\alpha = 0$.

2.4 Contributions

In earlier works, the configuration in which the vibrations were applied consisted of one vibrating surface and an object on top that can freely move vertically and levitate [16][23]. The increase in interfacial separation causes fewer asperities to remain in contact, so friction is significantly decreased, as discussed earlier.

Now, we are interested to find out if friction can also be increased if we use the squeeze film as a pushing force to bring two other surfaces closer together. We hypothesize that by introducing an extra constraint, a fixed layer on top of the object that was touching the vibrating surface, we should be able to both increase and decrease friction. This paper therefore presents two models (for vibrations from 1 and 2 sides) of the friction force over vibration amplitude, initial compression, and surface roughness for this

new configuration. Moreover, two test set-ups are built, by which the predictions of the model can be validated experimentally.

3 MODEL FRICTION MODULATION

We study two scenarios in which vibrations are applied, either from one or both sides, also resulting in two different models with their own force balance. F_e is the externally applied load force, and F_N is the normal force. F_r is the reaction force of the remaining asperities in contact, derived from Persson's theory of contact (Eq. 1). F_a is the force generated by the squeeze film, derived from Reynolds theory (Eq. 4). Lastly, F_s is the reaction force that arises from the compression of the soft material layer in between. In this study, the soft middle material layer is very light ($mg \ll F_e, F_a, F_r$), which is why the gravitational forces that arise from the masses are neglected. The forces F_e, F_a, and F_r can be obtained by multiplying the corresponding pressure (p_e, p_a, p_r from Eq. 1 and 4) times their area of contact A.

Fig. 4 depicts the force balances for our configuration. As the soft material layer changes its reaction force linearly with u_{top} and u_{bottom}, the layer is visualized and modelled as a linear spring with $F_s = -kdL$. Here, the stiffness of the layer k is given by $k = EA/L_0$, with E being the Young's modulus of the material, A the area of contact, and L_0 the thickness of the layer without compression. The change in thickness dL is given by $dL = L_0 F_e / AE$, where F_e is the external load force. In the figure, the gap between the soft material layer and the outer surfaces is visualized as a non-linear spring. This spring is added to show that this gap is not empty, but there are reaction forces present due to the interaction of the remaining asperities in contact and the impedance the squeeze film. Nonetheless, for the calculations of the reaction forces that arise from this non-linear spring,
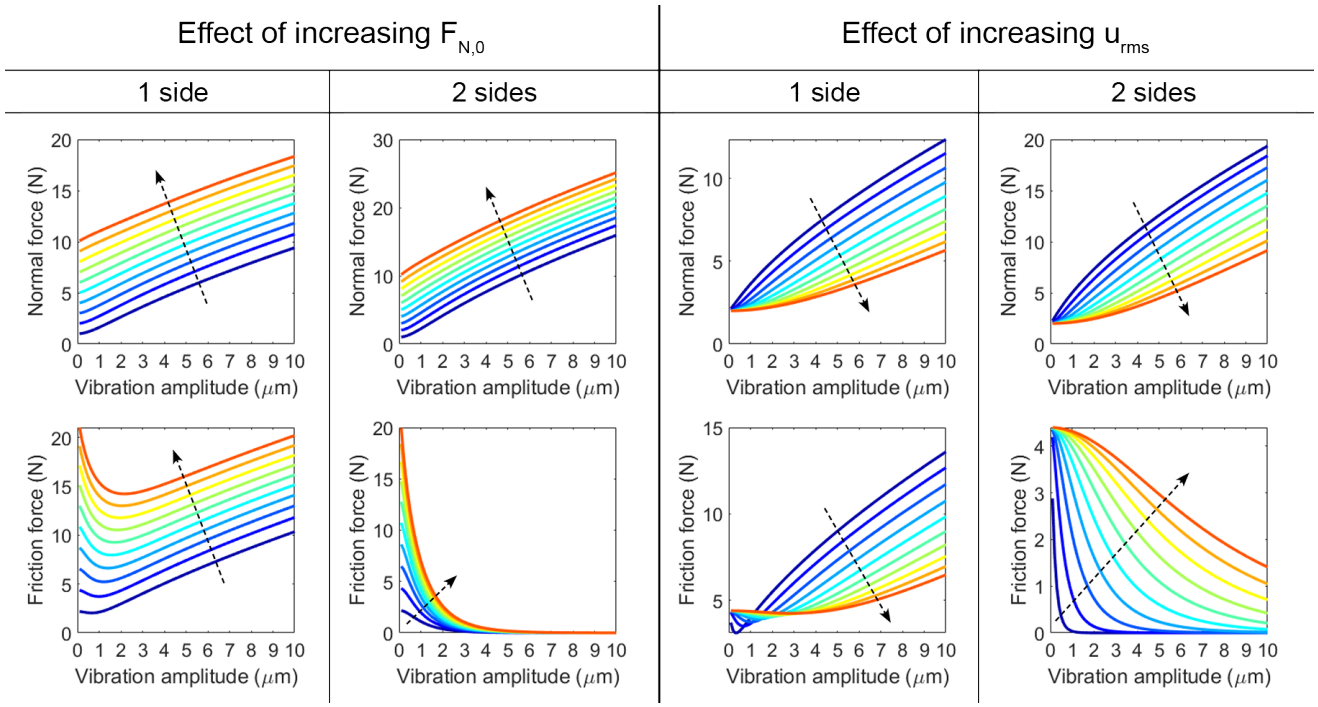
Fig. 5. Simulation results: effect of various initial compression forces ($F_{N,0}$), surface roughness (u_{rms}), and changing vibration amplitude (α), on normal and friction force. Colors: blue low values for $F_{N,0}$ and u_{rms}, and red high ones, also indicated by the arrow.

we do not calculate the spring's stiffness itself (as it is non-linear this is difficult to obtain), but instead we directly substitute the forces F_r and F_a that we obtained from Eq. 1 and 4 into the force balance.

3.1 Model 1 - Vibrations from 1 side

For the situation where vibrations are applied only on one side of the soft material layer (see Fig. 4b.), we have four force balance equations, from top to bottom, following from the static equilibrium equations of surfaces being in contact:

$$F_e = F_{r,top} + F_a, \tag{7}$$

$$F_s = F_{r,top} + F_a, \tag{8}$$

$$F_s = F_{r,bottom}, \tag{9}$$

$$F_N = F_{r,bottom}. \tag{10}$$

When we substitute the forces F_a, $F_{r,top}$, $F_{r,bottom}$, and F_s, this leads to the following equations:

$$F_e = Ap_c exp\left(\frac{-u_{top}}{u_{rms}}\right) + A\frac{5}{4}p_0\frac{\alpha^2}{u_{top}^2}, \tag{11}$$

$$F_s = Ap_c exp\left(\frac{-u_{top}}{u_{rms}}\right) + A\frac{5}{4}p_0\frac{\alpha^2}{u_{top}^2}, \tag{12}$$

$$F_s = Ap_c exp\left(\frac{-u_{bottom}}{u_{rms}}\right), \tag{13}$$

$$F_N = Ap_c exp\left(\frac{-u_{bottom}}{u_{rms}}\right). \tag{14}$$

Ultimately, the goal of the model is to be able to express u_{top} and u_{bottom} in terms of the initial compression force $F_{N,0}$, the vibration amplitude α, and the surface roughness u_{rms}, as these are independent variables that can be controlled in the real experiment. Variables u_{top} and u_{bottom} are the most important dependent variables to analyse, as these variables determine the total friction force. Moreover, we are also interested in analysing the effect of varying variables on F_N, to be able to make an estimate on how much additional force is added by the acoustic squeeze film.

For obtaining a relationship for u_{top}, u_{bottom}, and F_N, we can rewrite Eq. 11-14 into a set of two equations that depend both on u_{top}, u_{bottom}, and F_N:

$$F_N = A\left[p_c exp\left(\frac{-u_{top}}{u_{rms}}\right) + \frac{5}{4}p_0\frac{\alpha^2}{u_{top}^2}\right] \tag{15}$$

$$F_N = Ap_c exp\left(\frac{-u_{bottom}}{u_{rms}}\right) \tag{16}$$

However, to solve this system, we at least need one more equation so that the unknowns (u_{top}, u_{bottom}, and F_N) are balanced by the number of equations. Therefore we introduce two constraint equations. The first constraint follows from the relative distance between the outer surfaces. This distance is controlled in the experiment and does not change when vibrations are applied. Therefore we assume that the total gap with and without squeeze film is constant (see Eq. 17). The second constraint describes the thickness of the soft material layer as a function of the elastic force (Eq. 18).

$$u_{top,0} + u_{rubber,0} + u_{bottom,0} = u_{top} + u_{rubber} + u_{bottom}, \quad (17)$$

$$u_{rubber} = L_0 - \frac{F_N L_0}{EA}. \quad (18)$$

Initially, no squeeze film is present, which simplifies the corresponding equations, enabling us to immediately calculate the initial forces and initial interfacial separation distances: Without a squeeze film, we know that applied external force equals the reaction force both on top and the bottom of the middle layer, the spring force in between, and the normal force down below ($F_{r,top} = F_{r,bottom} = F_{s,0} = F_{N,0}$). This initial force can be measured with a normal force sensor so is known. Furthermore, as the reaction force at the bottom and top are the same, we also know that the interfacial separation distance initially is the same ($u_{0,top} = u_{0,bottom} = u_{rms}ln(Ap_c/F_{N,0})$). Lastly, $u_{rubber,0}$ can be obtained by Eq. 18. Substituting $u_{0,top}, u_{0,bottom}$ and $u_{rubber,0}$ into Eq. 17 leads to:

$$2\left[u_{rms}ln\left(\frac{Ap_c}{F_{N,0}}\right)\right] + \left[L_0 - \frac{F_{N,0}L_0}{EA}\right] = \quad (19)$$
$$u_{top} + u_{rubber} + u_{bottom}.$$

Regarding the variables with a squeeze film present, we are now left with four unknown variables (F_N, u_{top}, u_{rubber}, and u_{bottom}) and four equations depending only on these variables (Eq. 15, 16, 18, and 19), so that we can solve the system of equations numerically. In this study, we solved the system of equations with the *vpasolve* algorithm of MATLAB 2020a.

We already derived the friction as a function of u_{top} and u_{bottom} in Eq. 3. In our setup, the total friction force is the sum of the friction between the top surface and the soft middle layer and the bottom surface and the soft middle layer. If we substitute the values we found for u_{top} and u_{bottom} in Eq. 3, we can therefore find the total friction force $F_{f,tot}$ as:

$$F_{f,tot} = F_f(u_{top}) + F_f(u_{bottom}) \quad (20)$$

$$F_{f,tot} = F_{f,0}\left[exp\left(\frac{-u_{top} + u_0}{u_{rms}}\right) + exp\left(\frac{-u_{bottom} + u_0}{u_{rms}}\right)\right] \quad (21)$$

3.2 Model 2 - Vibrations 2 sides

The model with vibrations from two sides is a simplified version of the model with vibrations from one side. As we assume symmetric vibrations on both sides, we also expect a symmetric squeeze film and compression behaviour around the mid-line of the soft middle layer. Practically this means that u_{top} is always equal to u_{bottom}. Therefore we can consider only the top part for analysis. For the thickness of the middle layer we calculate half the thickness (changing Eq. 18 into Eq. 22). Furthermore, the gap width constraint also only needs to be concerned with the upper part (changing Eq. 17 and 19 into 23 and 24).

$$u_{rubber} = 1/2\left(L_0 - \frac{F_N L_0}{EA}\right), \quad (22)$$

$$u_{top,0} + u_{rubber,0} = u_{top} + u_{rubber}, \quad (23)$$

$$\left[u_{rms}ln\left(\frac{Ap_c}{F_{N,0}}\right)\right] + \left[L_0 - \frac{F_{N,0}L_0}{EA}\right] = u_{top} + u_{rubber}. \quad (24)$$

Now we are left with three unknowns (u_{top}, u_{rubber}, and F_N), and three equations (Eq. 15 22, and 24), so the system can again be solved numerically.

The total friction force is now twice the friction at the top (as we assumed symmetry). We can therefore substitute our calculated u_{top} in Eq. 3, so that we get:

$$F_{f,tot} = 2F_f(u_{top}). \quad (25)$$

$$F_{f,tot} = 2\left[F_{f,0}exp\left(\frac{-u_{top} + u_0}{u_{rms}}\right)\right]. \quad (26)$$

3.3 Numerical results

Fig. 5 visualizes the prediction of the model for varying the vibration amplitude α, the initial compression force $F_{N,0}$, and the surface roughness u_{rms}, on both the normal force and friction force. In general, the model predicts that the higher the vibration amplitude, the larger the expected normal force. The model therefore appears to confirm our initial intuition that an increase in vibration amplitude correlates with larger squeeze film forces.

Furthermore the model with vibrations from 1 side predicts that the friction force will increase. This outcome strengthens our hypothesis about the squeeze film force increasing the gap on the vibration side, and decreasing it on the opposite side, so that the total friction force can be increased.

In the model results for 2 sided vibrations, we observe that the model predicts a significant decrease in friction. This prediction too, confirms our expectations that a squeeze film on both sides can be used to decrease friction.

Regarding the effect of initial compression and surface roughness, we observe a general trend that the largest differences in friction and normal force are achieved with high compression forces and smooth surfaces. Also this prediction we can understand intuitively by considering the interfacial separation to be smaller for higher compression forces or with smoother surfaces. The smaller the interfacial separation, the higher the squeeze film pressure that can arise (according to Eq. 4), so probably also the larger the force differences that we observe.

4 MATERIALS

4.1 Hardware

We developed two test set-ups (depicted in Fig. 6): one set-up for experiments with vibrations from 1 side and another for experiments with vibrations from 2 sides. Both set-ups are built upon two aluminium breadboards of 300x600x12.7 mm with M6 taps (MB3060/M, Thorlabs) to ensure a rigid foundation. Attached to the upward breadboard is a 25 mm Travel Translation micrometer stage that can make discrete steps of 10 micrometer (XR25C, Thorlabs). Two right-angle brackets with a 25 mm diameter hole (CAM1/M, Thorlabs) are used to hold the transducers and their amplifying cones. By translating the micrometer stage and the components attached to it vertically, we can set a certain amount of initial compression in the experiments.

For the soft middle layer, we used three rubber plates of 60x40x1.5 mm each. In set-up 1, the rubber plate is placed between the amplifying cone and a steel plate that is attached to the normal force sensor, and in set-up 2, the rubber is placed between the two amplifying cones. We choose rubber because this material is elastic enough to test different compression levels, but stiff enough to not immediately stretch while being pulled. Because we want to test three different roughness levels, we rubbed two of the rubber plates with sandpaper of two different grit sizes according to a procedure explained in Appendix E. This resulted in three roughness levels of $u_{rms} = 1.5\mu m$, $u_{rms} = 4.4\mu m$, and $u_{rms} = 8.2\mu m$.

Pulling of the rubber layer is accomplished by a linear positioning stage (M-505.4DG Linear Positioning Stage, Physik Instrumente (PI)), that can translate horizontally with a speed of 1 mm/s. The rubber plate is glued to a 3D printed part that can be rigidly connected to the PI stage by an M3 threaded rod, so that the plate is being pulled uniformly.

Ultrasonic vibrations are generated by two Mini Bolt Clamped Langevin Transducers (SMBLTF40W25, Stemnic). The sine waves for actuation of the Langevin transducers are generated with a function generator (Analog Discovery 2, Digilent), with an output voltage up to $+/- 3$ V. By means of a Laser Doppler Vibrometer (LDV)(Polytec, OFV505) we found resonance frequencies of 38.57 kHz and 38.31 kHz for the top and bottom transducer respectively (procedure explained in Appendix B). For the 2 sided vibration experiment, we used the average of both frequencies (38.44 kHz) and the same phase. The signal is then amplified via High Voltage Amplifiers (High Voltage Amplifier DC - 5MHz, Falco Systems WMA-300) that provide an amplification factor of 50, thus an output voltage of $+/- 150$ V. Two horns with a diameter of 22 mm, clamp the Langevins to the base of the set-up without dampening the vibrations, and amplify the vibration amplitudes. The transducers

a. Vibrations 1 side   b. Vibrations 2 sides

c. Linear positioning stage
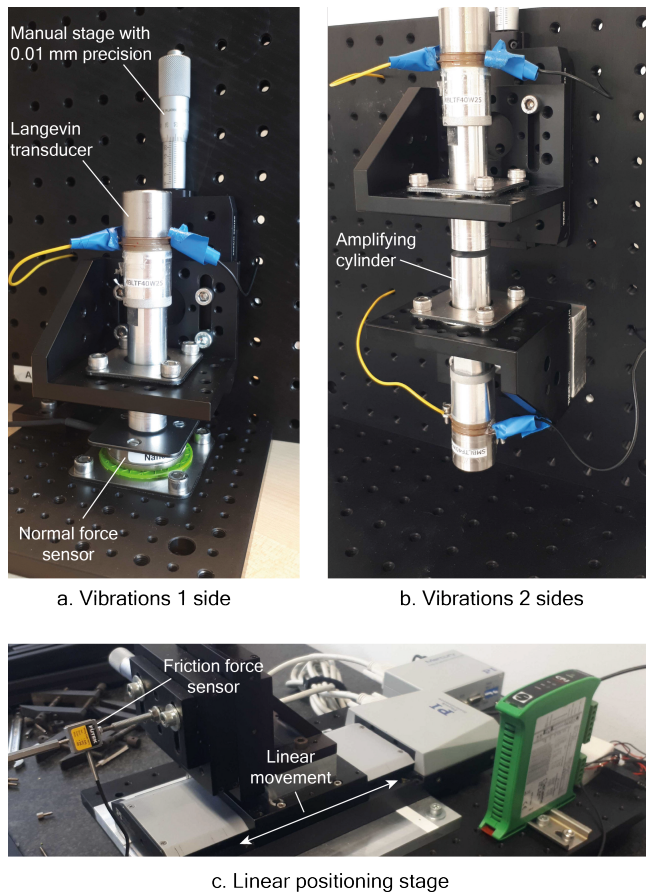
Fig. 6. Set-ups for both experiments. Soft material layer would be placed in between Langevin cone and normal force sensor or between the two amplifying cones. The rubber layer is rigidly connected to a linear positioning stage, that can pull the layer from between the cone and sensor, or two cones.

provide a piston-like vibrating motion so that the whole area is vibrated in the same way, and a uniform squeeze film can be generated.

In set-up 1 both the normal and friction force are measured. In set-up 2 only the friction force, due to lack of space for a normal force sensor. The normal force is measured via a 6 axis load cell (Nano45 SI-9-0.125, ATI Industrial Automation Inc., Apex, NC, USA). The sensor has a sensing range up to 9N and a resolution of 1/512N in the vertical direction. It needs to be calibrated before each trial. For the friction force, a miniature S-beam 10N load cell (LSB200, Futek) was used. This load cell is attached to the PI linear stage.

5 EXPERIMENT

Four experiments are performed: two with vibrations from 1 side (set-up 1) and two with vibrations from 2 sides (set-up 2). Per set-up, we test the effect of initial compression and surface roughness on the normal and friction force. Moreover, in each experiment, we also test the effect of changing vibration amplitude on normal and friction force.
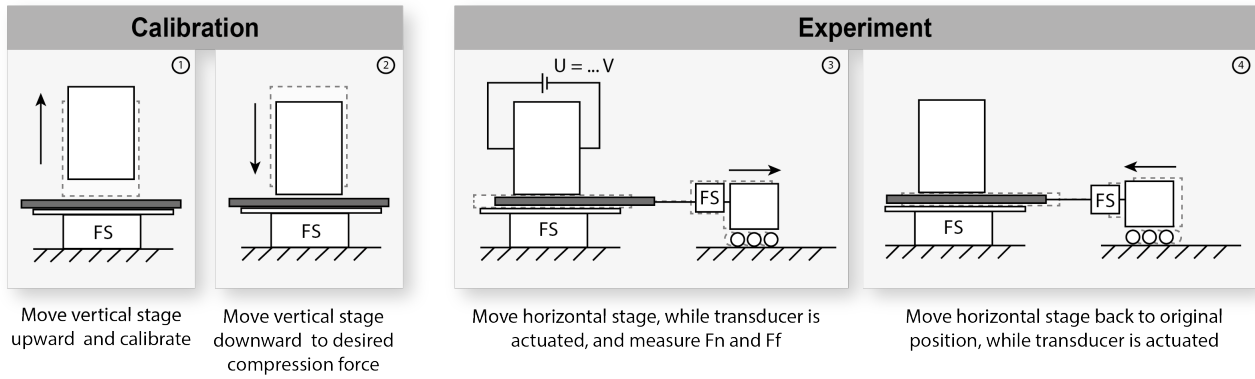
Fig. 7. Experimental procedure for experiments with vibrations from 1 side: First two steps are calibration steps, after which the experiment is performed in step 3 and 4. In the experiment, step 3 and 4 are repeated 7 times, each time for a different voltage input: $U = [0; 25; 50; 75; 100; 125; 150]V$. For the experiments with 2 side vibrations, the normal force sensor is replaced by another transducer.

5.1 Vibrations 1 side

For the experiment with vibrations from one side, the following steps are conducted (see also Fig. 7):

1) **Calibration:** Manual stage moved upward so there is no contact between the cone and the rubber layer. Now the normal force sensor is calibrated for zero compression.

2) **Finding the correct position:** Stage moved downward while measuring normal force until the desired initial normal force has been reached. The current position of the manual stage remains the same for this repetition, and only the vibration amplitude is varied.

3) **First measurement:** The horizontal stage pulls the rubber layer from between the cone and normal force sensor for about 21 seconds, in which the horizontal stage translates 2 cm at the speed of 0.1 cm/s, while continuously measuring both the normal force as well as the friction force. In this first run, no Voltage is applied to the Langevin transducer so that zero vibration amplitude is achieved.

4) **Vary vibration amplitude:** After the previous measurement, the horizontal stage translates back to its original position, from where the second measurement is started. This time, the Langevin is excited at 50 V. This process is repeated seven times, each time for a different voltage input: [0 25 50 75 100 125 150] V. This ends the first set of measurements.

5.2 Vibrations 2 sides

For the two-sided experiment, the normal force is not measured, only the friction force, as there is no room for a normal force sensor in the set-up. Therefore steps 1 and 2 are different from those above: during step 1, the stage is moved upwards, but without calibrating anything. In the second step, we move the stage downwards, but instead of inspecting the normal force, we inspect the friction force and set the vertical stage to the desired position when a certain friction force level has been met. Steps 3 to 5 are similar to the experiment with vibrations from 1 side.

5.3 Pilot experiment

As the normal and friction force are measured over time, a pilot experiment was performed to analyse how much time it took for the normal and friction force data to saturate. We found that it took between 5-8 seconds for the force data to reach a steady state, and we, therefore, decided to analyse the last 10 seconds out of 21 s from each measurement repetition, both for the normal as well as for the friction force (see Appendix D for details).

6 RESULTS

Four experiments have been performed: a change in $F_{N,0}$ and u_{rms} both for 1 side vibrations and 2 side vibrations. Both for the experiments where we varied $F_{N,0}$ and u_{rms}, we obtained three different plots: one normal force and friction force plot with vibrations from 1 side, and one friction force plot with vibrations from 2 sides, as only the friction force could be measured during those experiments. In this section, we first discuss the results of a change in $F_{N,0}$, and secondly, the change in u_{rms}.

The raw data can be found in Appendix D. Per repetition (one time sliding back and forth for a given initial compression and vibration amplitude), the mean force is calculated, which results in one data point. The curves in Fig. 8 and 10 are the result of different repetitions with the same initial compression, but with different vibration amplitudes.

As there are many different parameters involved in generating a squeeze film, it is hardly impossible to get each parameter the same in the model as in reality. Therefore we choose to compare our measurements to the general trends of the model rather than to the absolute predictions of the model. Nonetheless we believe that a comparison to the general trends can already provide a clear inside on how well the model predicts reality.

(a) Normal force   **(b)** Friction force
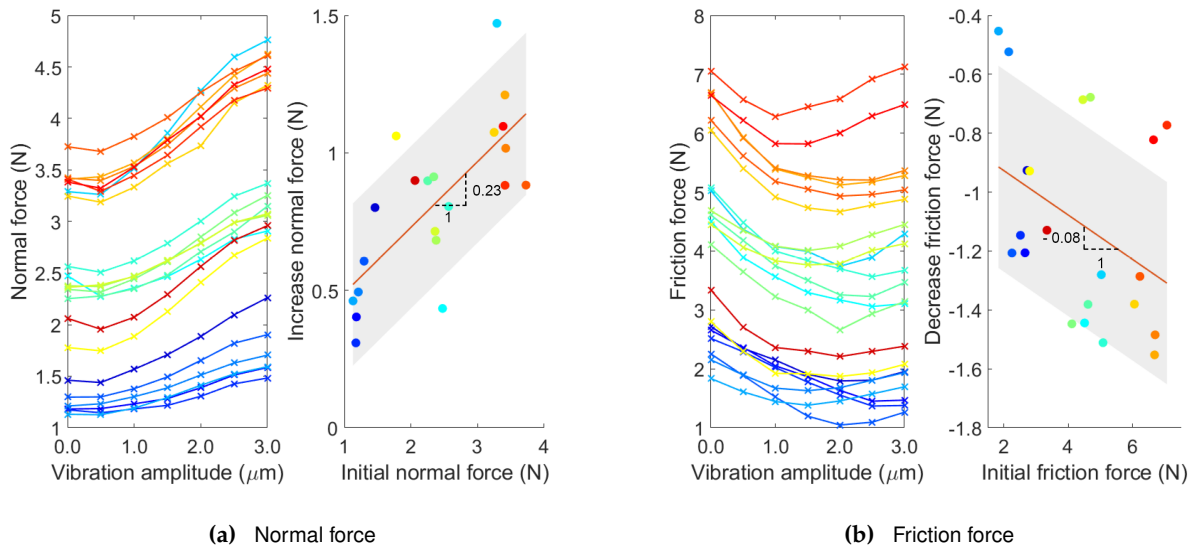
Fig. 8.   **Experiment 1 side vibrations - vary initial compression:** Left plots in **a.** and **b.** show change in normal and friction force over vibration amplitude (α) and initial compression ($F_{N,0}$). Colors represent chronology of measurements (blue is first, red is last). Grey shade visualizes std. Right plot in **a.** depicts linear regression of the increase in normal force between $\alpha = 0\mu m$ and $\alpha = 3\mu m$ over the initial normal force, and right plot in **b.** the linear regression of the decrease in friction force between $\alpha = 0\mu m$ and the minimal friction force.

6.1 Effect of initial compression

The results of a change in initial compression are depicted in Fig. 8 (experiment vibrations 1 side) and Fig. 9 (experiment vibrations 2 side). The normal force could only be measured during the experiments with vibrations from 1 side, resulting in two plots in Fig. 8 and only one in Fig.9.

6.1.1 Normal force - 1 side vibrations

Fig. 8a shows 21 repetitions of normal force measurements for varying vibration amplitude at different initial compression forces. The force increases both with increasing vibration amplitude and compression force, similar to the predictions from the model. A simple regression ($y = ax + b$) revealed a trendline with coefficients $a = 0.23$ and $b = 0.25$. This trend indicates that the increase in normal force is larger for higher initial compression forces than for lower ones.

The trend contradicts the model's predictions, which showed a similar normal force increase between different compression levels. We first suspected this difference could be caused by a drift of the normal force sensor. However, after analysis (outlined in Appendix F), this drift didn't seem to be significant. Another explanation for this disagreement might be that for lower initial compression forces, the interfacial separation u between the surfaces was larger than we predicted. Thus the squeeze number could have been lower than we predicted. Zhao et al. found that for squeeze numbers $\sigma < 100$, Rayleigh's acoustic radiation theory better approximates reality than Reynold's lubrication theory. The theory of Rayleigh also predicts less pressure being built up in the squeeze film compared to Reynold's theory. Looking back at our calculations for the squeeze number,

we assumed u to be in the order of 10^{-5} m. If the interfacial separation, in reality, was even smaller, the squeeze number would be higher than calculated, and Reynold's theory was the correct model. However, if the gap was, in reality, larger than this 10^{-5} m, the squeeze number would have been smaller. In fact, if u would have been a factor 3 larger than the assumed 10^{-5} m, that could already result in a squeeze number $\sigma < 100$. This uncertainty about the exact value of u explain the difference in force increase between small and higher compression forces.

6.1.2 Friction force - 1 side vibrations

Fig. 8b shows 21 repetitions of friction force measurements corresponding to the normal force data from Fig. 8a for varying vibration amplitude and initial compression. As the model predicted, a larger dip in force for higher compression forces, we checked this with a simple linear regression over the difference in friction force at $\alpha = 0\mu m$ and the minimal friction force plotted against the initial friction force. A trendline with coefficients $a = -0.08$ and $b = -0.76$ revealed that the decrease in friction force is indeed larger for a higher initial compression compared to a lower initial compression forces.

Moreover, the model predicted an increase in friction force for higher vibration amplitudes. We tested this as well. A one-sample t-test over the difference in the minimal friction force value and friction force value at $\alpha = 3\mu m$, with null-hypothesis a mean of zero increase, revealed a significant main effect ($Mean = 0.2746, STD = 0.2170, p < 0.0001$). The significant increase in friction force contributes to the hypothesis that the squeeze film can be used as a force to push the middle layer more closely toward the opposite surface, so that friction is increased there.

6.1.3 Friction force - 2 side vibrations

Fig. 9 shows 16 repetitions of friction force measurements for varying vibration amplitude at different initial compression forces. The main trend is similar between the model and the measurements: the total friction force decreases significantly over vibration amplitude. This trend indicates that it is possible with the current set-up to generate a squeeze film on both sides within a confined space.
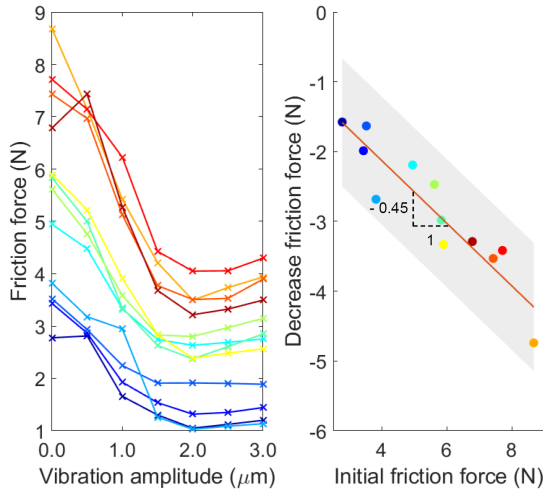
Fig. 9. **Experiment 2 side vibrations - vary initial compression:** Left plot shows change in friction force over vibration amplitude (α) and initial compression ($F_{N,0}$). Colors represent chronology of measurements (blue is first, red is last). Grey shade visualizes std. Right plot depicts the linear regression of the decrease in friction force between $\alpha = 0\mu m$ and $\alpha = 3\mu m$ over the initial friction force.

One disagreement between the model and results is the prediction of saturated friction force. The model predicted that this saturation would be at a friction force of $0N$, independent of the initial compression. Though, we observe that higher initial compression yields a higher saturation force. This non-zero saturation force implies that the higher the initial compression, the more difficult it is to entirely lose contact between the surfaces. Intuitively this assumption is correct, as a higher initial compression means that the surfaces are more closely together. Thus more asperities make intimate contact. To be able to entirely break this contact, there has to be enough space, which is not the case for high compression forces.

Furthermore, the model predicted a larger difference between the initial force and the saturation level for higher initial compression. To confirm this result we obtained a simple linear regression, which resulted in a trendline with coefficients $a = -0.45$ and $b = -0.34$. Thus the measurements are in line with the model. An explanation for the larger force difference for higher initial compression forces is that for higher forces the gap is smaller. Therefore, more squeeze film pressure can be built up, thus relatively

more asperities lose contact compared to situations with lower initial compression forces.

The last thing we tested for this experiment was if the friction force also showed an increase in force for the higher vibration amplitudes. At first glance, the friction force remains constant once it reaches a steady state. However, when we zoom into the data, we notice that most curves follow a somewhat increasing trend for the higher vibration amplitudes. We tested the significance of this observation with a one-sample t-test over the difference in the minimal friction force value and friction force value at $\alpha = 3\mu m$. The test revealed indeed a significant increase ($p < 0.0003$) in force ($Mean = 0.2380, STD = 0.1493$). Note that this increase is of the same order as for the experiment with vibrations from one side, which makes it an interesting point of discussion.

6.2 Effect of surface roughness

6.2.1 Normal force - 1 side vibrations

Fig. 10a shows 18 repetitions of normal force measurements for varying vibration amplitude and three surface roughness levels ($u_{rms} = 1.5\mu m$, $u_{rms} = 4.4\mu m$, and $u_{rms} = 8.2\mu m$). The force increases with vibration amplitude, similar to the predictions of the model. As the model also predicted, we find a smaller increase in normal force for layers with a higher roughness: the boxplots on the right show that the increase in normal force between $\alpha = 0\mu m$ and $\alpha = 3\mu m$. The largest difference is found for the smoothest layer (layer 1) with roughness $u_{rms} = 1.5\mu m$ ($Mean = 0.74, STD = 0.18$). The second largest difference was found for the second smoothest layer (layer 2) with roughness $u_{rms} = 4.4\mu m$ ($Mean = 0.64, STD = 0.07$). The smallest force difference was found for the roughest layer (layer 3) with $u_{rms} = 8.2\mu m$ ($Mean = 0.50, STD = 0.09$). An independent t-test revealed no significant effect between layer 1 and 2 ($p > 0.05$), but does show a significant difference between layer 1 and 3 ($p < 0.02$), and between layer 2 and 3 ($p < 0.02$).

Nevertheless, when studying Fig. 10a, it seems that one of the reasons that the increase in normal force is less significant for the rougher surfaces compared to the smoother surfaces is that the rougher surfaces experience a dip in friction force between $\alpha = 0-3\mu m$. The gradients of the higher amplitudes seem very similar. This dip in normal force is an interesting effect that the model did not predict. According to the model, F_N could only increase for higher vibration amplitudes, which intuitively makes sense as the squeeze film that arises accounts for a higher pressure in the gap, thus also a higher measured normal force. Since the decrease in normal force contradicts our intuition, we will address this in more depth in the discussion section.

(a) Normal force   **(b)** Friction force
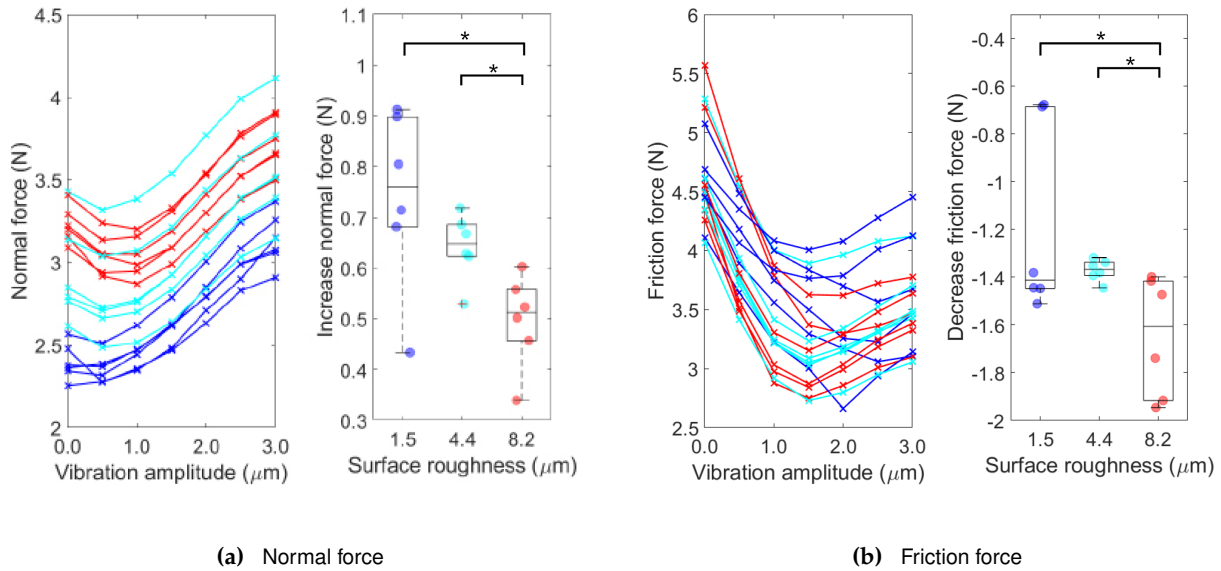
Fig. 10. **Experiment 1 side vibrations - vary surface roughness:** Left plots in **a.** and **b.** show change in normal and friction force over vibration amplitude (α) and surface roughness (u_{rms}). Colors represent three levels of roughness. The right plot in **a.** depicts the increase in normal force between $\alpha = 0\mu m$ and $\alpha = 3\mu m$ for each roughness level. The right plot in **b.** depicts the decrease in friction force between $\alpha = 0\mu m$ and the minimal friction force. Significant difference ($p < 0.05$) indicated by $*$.

6.2.2 Friction force - 1 side vibrations

Fig. 10b shows 18 repetitions of friction force measurements for varying vibration amplitude and surface roughness. The figure, clearly shows the decrease and increase in friction force over vibration amplitude, as predicted by the model. With a one-sample t-test, we checked the significance of the force increase between the minimal friction force value and friction force value at $\alpha = 3\mu m$. The null hypothesis would be a mean of zero increase. The test revealed a significant main effect ($Mean = 0.3368, STD = 0.1464, p < 0.0001$).

Furthermore, the model predicted that a lower surface roughness would result in a larger dip in friction force. We studied similarities between this prediction and the measurements with the boxplots on the right. The boxplots show that the decrease in friction force at $\alpha = 0\mu m$, and the friction force at its minimum are smallest for layer 1 ($Mean = -1.19, STD = 0.40$), medium large for layer 2 ($Mean = -1.37, STD = 0.05$), and largest for layer 3 ($Mean = -1.65, STD = 0.25$). An independent t-test reveals no significant effect between layer 1 and 2 ($p > 0.05$), but does show a significant difference between layer 1 and layer 3 ($p < 0.04$) and between layer 2 and layer 3 ($p < 0.03$). These results seem to contradict the predictions by the model, as rougher surfaces show a larger dip in friction force. We expect that the disagreements between model and results might not be a fault in the model but rather that other hidden parameters in the set-up accounted for the increase in force. More details about our interpretation of the causes of this disagreement can be found in the discussion section.

6.2.3 Friction force - 2 side vibrations

Fig. 11 shows 17 repetitions (18 performed, 1 wrongly recorded) of the friction force measurement for varying vibration amplitude and surface roughness. The friction force decreases over vibration amplitude and saturates at some point, in correspondence to the predictions by the model. Only here as well, the saturation force is a non-zero force.

Furthermore, the model predicted a steeper decay in friction force for less rough surfaces. We checked this by calculating the gradient of each curve between $\alpha = 0\mu m$ and $\alpha = 1\mu m$ (the part where it is still decaying) and plotted these results in three separate boxplots on the right. The curve is least steep for layer 1 ($Mean = -2.07, STD = 0.32$), for layer 2 ($Mean = -2.31, STD = 0.22$), and steepest for layer 3 ($Mean = -2.60, STD = 0.35$). An independent t-test revealed only a significant main effect between layer 1 and layer 3 ($p < 0.03$). Between layer 1 and 2, and layer 2 and 3 no significant difference could be demonstrated (both $p > 0.05$). These results counteract the model's predictions, as it at shows a steeper decay for rougher surfaces. We expect that the disagreements between the model and results might not be a fault in the model but that there are other hidden parameters in the set-up that accounted for this force. More details about our interpretation of the causes of this disagreement can be found in the discussion section.

Also, for this experiment, we checked whether there was a significant increase in force for the higher vibration amplitudes. A one sample t-test over the difference in the minimal friction force value and friction force value at $\alpha = 3\mu m$, revealed that there is

indeed a significant main effect ($p < 0.0001$) in force increase ($Mean = 0.2643, STD = 0.1571$).
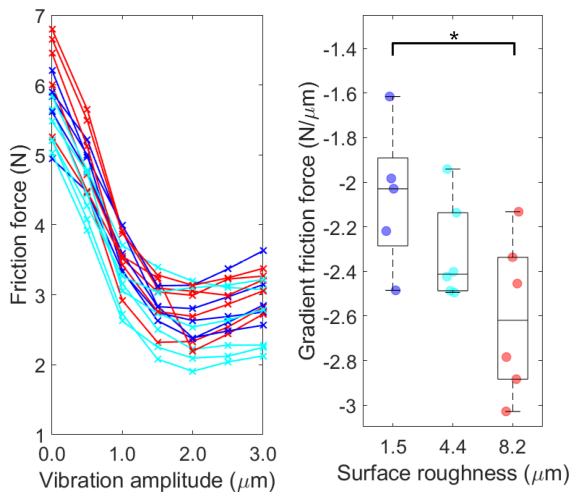
Fig. 11.   Experiment 2 side vibrations - vary surface roughness: Left plot shows change in friction force over vibration amplitude (α) and surface roughness (u_{rms}). Colors represent three levels of roughness. The right figure depicts the gradient of the friction decrease between $\alpha = 0\mu m$ and $\alpha = 1\mu m$ for each roughness level. Significant difference ($p < 0.05$) indicated by $*$.

7 DISCUSSION

In earlier works, the squeeze film effect has been implemented to levitate objects and, in this way, reduce friction. This study shows that a squeeze film can also arise when the object on top is not free to levitate. With the current method, the squeeze film effect can both be implemented to decrease and increase friction. Being able to increase friction on command, can be useful in blocking mechanisms, as you would only have to actuate your device when a blocking action is required. On the other hand, a mechanism that decreases friction once actuated, has to be actuated all the time when no blocking is wanted, and be turned off when a blocking action is required. This friction-decrease mechanism is still useful, but less energy efficient than the friction-increase mechanism.

We will now discuss our interpretation about what mechanism is responsible for the increase and decrease in friction between the surfaces for vibrations from 1 and 2 sides.

7.1 Squeeze film in a confined space

In Fig. 8a, we observed that the normal force increases over increasing vibration amplitude. When the transducers start vibrating, we can imagine that there are two factors influencing the normal force. On the one hand, there are the transducers themselves, which quickly expand and shrink within each oscillation cycle. During expansion, they result in an additional compression force, of which the value depends on the amplitude of oscillation. However, as they also

shrink within each oscillation cycle, we expect that the time-averaged additional compression force is zero. On the other hand, the air in between the surfaces can start behaving like a trapped fluid, a squeeze film, causing an over-pressure in the gap that accounts for the increase in normal force. To find out which of these phenomena is occurring, we can take a look at Fig. 9. In this figure, we find that when vibrations are applied from 2 sides, the friction force significantly decreases over increasing vibration amplitude. This decrease in friction force indicates that a squeeze film must be present. Namely, if the increase in normal force would be purely because of the extra compression by the transducers, we would expect more asperities to be in intimate contact, thus an increase in friction over vibration amplitude. Since friction only decreases, air pressure must play a role.

We expect the squeeze film to compress the softer layer in between so that the asperities of the opposing surfaces release contact. However, there is a limit by which the soft layer can be compressed. The higher the initial compression, the more difficult it is to lose contact entirely between the asperities. This behavior can also be observed in Fig.9: higher saturation forces correlate to larger higher compression forces.

7.2 Friction modulation

7.2.1 Decrease friction

A decrease in friction can be achieved with vibrations from two sides, where higher vibration amplitudes result in less friction. Yet, there is a point at which the friction reaches a steady state. Physically the steady state is where no more asperities can release contact. We already mentioned that the higher the initial compression, the larger this saturation force. Additionally, we found that the higher the initial compression, the larger the decrease in friction force that can be achieved. An explanation for this larger decrease is that the smaller the initial gap, the higher the squeeze film pressure that will arise (as $p_a \propto 1/\alpha^2$). We conclude that there is a trade-off to be made when one's goal is to decrease friction: the higher the initial compression, the larger the absolute friction decrease that can be achieved, although the higher the force at which the friction saturates.

7.2.2 Increase friction

Increasing friction using the squeeze film effect is a principle that has never been studied. However, in this study, we showed that a significant increase in friction could be achieved for the highest vibration amplitudes, when vibrations were applied from one side and the other side is constrained (see Fig. 8b and 10b). This result strengthens the hypothesis that the squeeze film on one side causes the gap on the top to increase while the gap on the bottom decreases so that in the end the total friction increases.

Nonetheless, an observation in the experiment with 2 sided vibrations raises doubt about the working principle by which the friction increased: Although we expected in the experiment with vibrations from 2 sides that the friction force would only decrease, we find from Fig. 9 and 11 that in this experiment too, there is a small increase in friction for the higher amplitude ranges ($\alpha \approx 2 - 3\mu m$). The friction increase in the experiment with vibrations from 2 sides, is of the same order of magnitude as the friction increase in the experiment with vibrations from 1 side (note that the increase is not very clear from the figures, as these visualize a more zoomed-out picture, but statistics revealed that it is significant), indicating that there might be another cause for the increase in friction.
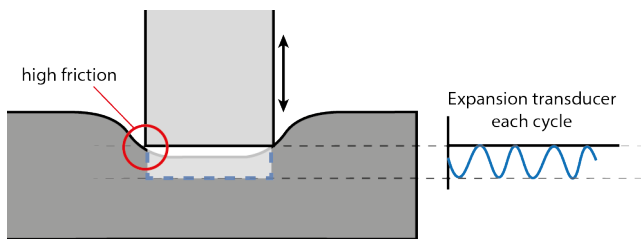
Fig. 12. Additional compression of middle layer due to expansion transducer might introduce higher friction on the edges of the transducer during each oscillation cycle.

One hypothesis that we currently have is that the increase in friction arises from extra resistance at the edges during compression (visualized in Fig. 12). When squeeze film compresses the soft layer, we assume that the compression only takes place at the location where the transducers and rubber make contact. At the edge of this contact area, the rubber transitions from a compressed position to its neutral position. Similar to when a fluid flows from a wider to a more narrow pipe, resistant forces arise at these edges. As this compression takes place both in the experiment with vibrations from 1 and 2 sides, this could be an acceptable explanation.

All things considered, we cannot be sure what the leading cause is for the increase in friction in either experiment. Therefore we have a list of recommendations for future research that might provide more insight into the exact working principle. First, we suggest designing a finite element model of the layer and transducers. This model can be used to estimate the resisting forces arising at the edges under compression. Secondly, a high-speed camera can capture the middle layer's deformation during the experiments. Furthermore, the test set-up can be altered in such a way that the area of the vibrating surface is larger than that of the soft material layer. This adjustment should result in no edge deformations but instead a uniform compression. If an increase in friction is measured in this configuration, it can only be attributed to the

asperities on the opposite surface being in more intimate contact. Moreover, the number of asperities in intimate contact, recalling the true area of contact, can even be measured [15]. Lastly, it might be interesting to find out what will happen at even higher vibration amplitudes, as in our set-up, we could not create amplitudes over $3\mu m$. Although the same problem could arise that we discussed before, that the transducers themselves account for the increase in friction force.

7.3 Surface roughness

It is generally known that surface roughness plays an essential role in friction behavior [24]. Therefore we were interested to find out what the effect of surface roughness was within our configuration. When we consider only two surfaces being in contact, we can imagine that the roughness of a surface largely determines the average interfacial separation. For a similar load force, we find that if both surfaces are very rough, the opposing asperities make earlier contact compared to when both surfaces are very smooth (visualized in Fig. 13). This difference in average separation explains two phenomena that also came forward in our model. Firstly, it means that because smooth surfaces are, on average, more closely together, that there is less room for the air molecules to move around. Thus, when vibrations are applied with these smooth surfaces, also the viscous forces in the squeeze film increase faster than with rougher surfaces. As the viscous forces are higher, also more pressure is generated, which explains the steeper increase in normal force in the model for smooth surfaces compared to rough surfaces (see model visualization Fig. 5). Secondly, smoother surfaces can easier reduce friction, as only a slight change in interfacial separation causes the opposing asperities to entirely lose contact. This behavior was also visualized in the model, where smoother surfaces show a steeper decay in friction force compared to rougher surfaces.
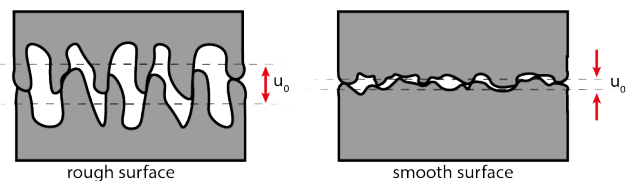
Fig. 13. For a similar external load force, rough and smooth surfaces have a different initial interfacial separation u_0.

7.3.1 Mismatch model and results

Nevertheless, when we look at the results from our measurements for varying surface roughness, we find an opposite behavior than predicted by the model: Rougher surfaces decrease in friction more (Fig. 10b) and faster (Fig. 11). This result means that either our model does not incorporate some very important surface roughness characteristics, or we had some hidden

variables without our set-up we did not account for. As our model's predictions agree with literature, we expect that the second argument is more likely to be true.

We hypothesize that the mismatch between model and results can be attributed to the alignment between the soft middle layer and the linear stage that pulls this layer from between the transducers. Within the roughness experiment, we had three different plates. Before each experiment, one of these plates had to be connected to the linear stage. When the plate was attached, we manually adjusted the height of the adjustment point at the linear stage, such that the layer stayed completely horizontal. Nonetheless, we confirmed this alignment by eye only, so there might have been some differences between the various plates that we used (depicted in Fig. 14). In retrospect, a slight misalignment of the middle layer might have introduced significant differences between layers. If there were forces pushing the middle layer downward, additional friction forces would also be present. Because of this uncertainty, we recommend redoing this experiment with a set-up where the alignment of the plates can be more accurately measured.
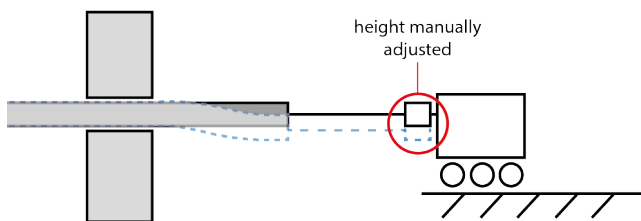
Fig. 14. The alignment between the middle layer and the linear stage was performed manually. If the alignment between the plates was slightly different between measurements, this could have caused a pre-tension on the plate that caused a higher friction force.

Regardless, the roughness experiments did highlight a phenomenon that we did not foresee: a slight dip in normal force over vibration amplitude, which is larger for the rougher surfaces. The dip is clearly visible in each of the repetitions, which makes it unlikely that it is due to measurement noise. Nonetheless, the result contradicts our intuition, as the squeeze film would intuitively only add an extra force to the force balance, and not remove it. Physically an explanation might be that there is some suction effect happening at this specific amplitude that causes the pressure in the gap to become lower than the ambient pressure, therefore reducing the measured normal force. To find out what working principle is responsible for this phenomenon, we recommend performing additional experiments with different surface roughness plates, and designing a finite element model that incorporates fluid dynamic equations. That way, we can find out how the pressure of the fluid changes with surface roughness.

7.4 Applicability for wearables

Before being able to implement this mechanism in wearables, several aspects require more research. First of all, we believe that the ideal brake mechanism introduces high friction when actuated and low friction when not actuated, similar to our experiment with vibrations from 1 side. This mechanism would be more energy efficient than when the transducers are actuated all the time when moving the fingers, and are only turned off when their motion must be blocked. However, at this point, we noticed that it is difficult to obtain an increase in friction force that is several orders of magnitudes larger compared to the initial friction. Also, we are still not sure by what mechanism the friction increased. We do believe that playing around with certain variables, like the thickness of the middle layer, the elasticity and roughness of the material, could result in larger friction differences. An optimization study can provide insight on the effect of each parameter.

The decrease in friction force with vibrations from 2 sides, however, was much larger and might even be enough to provide the required force feedback in wearables. Nonetheless, for this configuration too, future research is required in terms of what absolute force difference is actually required for users to experience it as force feedback, and also how to miniaturize the set-up.

Lastly, our experiment with the difference in roughness also illustrated the importance of a robust set-up, as small changes in orientation already drastically affected the results. The need for robustness might become a challenge when implementing it in a wearable, as humans move their limbs frequently, so slight orientation changes can quickly occur. Nevertheless, if this need is known beforehand, it can be incorporated into the design criteria.

8 Conclusion

When a soft material layer is clamped between two surfaces vibrating at ultrasonic frequencies, friction can either be increased or decreased, depending on whether the vibrations are applied from only 1 side or both sides. The change in friction is facilitated by a squeeze film that arises on the side where vibrations are applied. The squeeze film increases the interfacial separation between the surfaces, which causes less asperities to be in intimate contact so that friction is reduced. If this squeeze film is generated on both sides, friction is reduced significantly. However, when the squeeze film is generated on only one side, it can be used as a pressing force to push the middle layer more closely to the opposite surface, increasing friction there. Since friction scales by the negative exponential of the interfacial separation, the decreased gap width has a more dominant effect on the friction force than the increase in gap width. The total friction

is the sum of the friction on the top and bottom. Therefore with a similar change in gap width on the top and bottom, the total friction force can be increased. This expected behavior is supported by the model presented in this study. The model, based on Persson's theory of contact and Reynolds' squeeze film theory, predicts that the largest force differences can be found for high vibration amplitudes.

In the experiments that we performed to confirm the predictions from the model, we varied the vibration amplitude, initial compression and surface roughness. For both set-ups, with vibrations from 1 and 2 sides, we concluded that our model is well capable of predicting the general trends of a change in friction due to a variation in vibration amplitude and initial compression. However, there were still some disagreements between the model and results, which can likely be attributed to misalignment problems in the set-up.

Even though there is still room for improvement, we were able to deliver a significant contribution to a small and lightweight blocking mechanism for wearables.

ACKNOWLEDGMENTS

REFERENCES

[1] R. Johansson, "Johansson Testing," 2011. [Online]. Available: https://youtu.be/0LfJ3M3Kn80

[2] R. Hinchet, V. Vechev, H. Shea, and O. Hilliges, "Dextres: Wearable haptic feedback for grasping in VR via a thin form-factor electrostatic brake," UIST 2018 - Proceedings of the 31st Annual ACM Symposium on User Interface Software and Technology, pp. 901–912, 2018.

[3] B. Noronha and D. Accoto, "Exoskeletal Devices for Hand Assistance and Rehabilitation: A Comprehensive Analysis of State-of-the-Art Technologies," IEEE Transactions on Medical Robotics and Bionics, vol. 3, no. 2, pp. 525–538, 2021.

[4] T. du Plessis, K. Djouani, and C. Oosthuizen, "A review of active hand exoskeletons for rehabilitation and assistance," Robotics, vol. 10, no. 1, 3 2021.

[5] Y. Park, I. Jo, J. Lee, and J. Bae, "WeHAPTIC: A Wearable Haptic interface for Accurate Position Tracking and Interactive force Control," Mechanism and Machine Theory, vol. 153, p. 104005, 2020. [Online]. Available: www.elsevier.com/locate/mechmachtheory

[6] D. Xu, Q. Wu, and Y. Zhu, "Development of a soft cable-driven hand exoskeleton for assisted rehabilitation training," Industrial Robot, vol. 48, no. 2, pp. 189–198, 2020.

[7] Y. Chen, Z. Yang, and Y. Wen, "A soft exoskeleton glove for hand bilateral training via surface EMG," Sensors (Switzerland), vol. 21, no. 2, pp. 1–18, 2021.

[8] N. Smaby, M. E. Johanson, B. Baker, D. E. Kenney, W. M. Murray, and V. R. Hentz, "Identification of key pinch forces required to complete functional tasks," Journal of Rehabilitation Research and Development, vol. 41, no. 2, pp. 215–223, 2004.

[9] Q. A. Boser, M. R. Dawson, J. S. Schofield, G. Y. Dziwenko, and J. S. Hebert, "Defining the design requirements for an assistive powered hand exoskeleton: A pilot explorative interview study and case series," Prosthetics and Orthotics International, 2020.

[10] Q. Meng, S. Xiang, and H. Yu, "Soft Robotic Hand Exoskeleton Systems: Review and Challenges Surrounding the Technology," vol. 86, no. Eame, pp. 186–190, 2017.

[11] D. J. Meyer, M. Wiertlewski, M. A. Peshkin, and J. E. Colgate, "Dynamics of ultrasonic and electrostatic friction modulation for rendering texture on haptic surfaces," IEEE Haptics Symposium, HAPTICS, pp. 63–67, 2014.

[12] C. Basdogan, F. Giraud, V. Levesque, and S. Choi, "A Review of Surface Haptics: Enabling Tactile Effects on Touch Surfaces," IEEE Transactions on Haptics, vol. 13, no. 3, pp. 450–470, 2020.

[13] T. Engel, A. Lechler, and A. Verl, "Sliding bearing with adjustable friction properties," CIRP Annals - Manufacturing Technology, vol. 65, no. 1, pp. 353–356, 2016. [Online]. Available: http://dx.doi.org/10.1016/j.cirp.2016.04.084

[14] S. Zhao, S. Mojrzisch, and J. Wallaschek, "An ultrasonic levitation journal bearing able to control spindle center position," Mechanical Systems and Signal Processing, vol. 36, no. 1, pp. 168–181, 3 2013. [Online]. Available: http://dx.doi.org/10.1016/j.ymssp.2012.05.006

[15] M. Wiertlewski, R. F. Friesen, and J. E. Colgate, "Partial squeeze film levitation modulates fingertip friction," Proceedings of the National Academy of Sciences of the United States of America, vol. 113, no. 33, pp. 9210–9215, 2016.

[16] R. F. Friesen, M. Wiertlewski, and J. E. Colgate, "The role of damping in ultrasonic friction reduction," IEEE Haptics Symposium, HAPTICS, vol. 2016-April, pp. 167–172, 2016.

[17] B. Bhushan, Tribology and Mechanics of Magnetic Storage Devices. Springer, New York, NY, 1996.

[18] J. A. Greenwood and J. B. P. Williamson, "Contact of Nominally Flat Surfaces. J. A. Greenwood and J. B. P. Williamson, Proc." Proc. Roy. Sot. (London),, vol. 5, no. 1442, p. 1967, 1967.

[19] B. N. Persson, "Relation between interfacial separation and load: A general theory of contact mechanics," Physical Review Letters, vol. 99, no. 12, pp. 1–4, 2007.

[20] E. Salbu, "Compressible Squeeze Films and Squeeze Bearings," J. Basic Eng., vol. 86, p. 355–366, 1964.

[21] B. T. Chu and R. E. Apfel, "Acoustic radiation pressure produced by a beam of sound," Journal of the Acoustical Society of America, vol. 72, no. 6, pp. 1673–1687, 1982.

[22] R. F. Friesen, M. Wiertlewski, M. A. Peshkin, and J. E. Colgate, "Bioinspired artificial fingertips that exhibit friction reduction when subjected to transverse ultrasonic vibrations," IEEE World Haptics Conference, WHC 2015, pp. 208–213, 2015.

[23] V. C. Kumar and I. M. Hutchings, "Reduction of the sliding friction of metals by the application of longitudinal or transverse ultrasonic vibration," Tribology International, vol. 37, no. 10, pp. 833–840, 2004.

[24] M. Sahin, C. S. Çetinarslan, and H. E. Akata, "Effect of surface roughness on friction coefficients during upsetting processes for different materials," Materials and Design, vol. 28, no. 2, pp. 633–640, 2007.

[25] A. W. Bush, R. D. Gibson, and T. R. Thomas, "The elastic contact of a rough surface," Wear, vol. 35, no. 1, pp. 87–111, 1975.

[26] S. Zhang, Y. Li, S. Li, Y. Wu, and J. Zeng, "Investigation of the nonlinear phenomena of a Langevin ultrasonic transducer caused by high applied voltage," Proceedings of the Institution of Mechanical Engineers, Part C: Journal of Mechanical Engineering Science, vol. 236, no. 2, pp. 873–885, 2022.

APPENDIX A
DERIVATION CONTACT AND FRICTION FORCE

Persson's theory of contact states that the pressure from the reaction of the support, p_r, is proportional to the negative exponential of the interfacial separation:

$$p_r = p_c exp\left(\frac{-u}{u_{rms}}\right). \tag{27}$$

The variable p_c is called the maximum absolute pressure given by $p_c = 0.375q_0 u_{rms}E/(1 - v^2)$ [19]. Here, q_0 is the scale at which the u_{rms} is determined, E the Young's modulus of the material, and v the Poisson ratio.

When no vibrations are present ($\alpha = 0$), p_r balances the external load force p_e. If we call the separation distance that corresponds to this initial condition u_0, we can appreciate that

$$p_e = p_c exp\left(\frac{-u0}{u_{rms}}\right). \tag{28}$$

If we move the exponential to the other side, we can express p_c in terms of p_e and the exponential term:

$$p_c = p_e exp\left(\frac{u0}{u_{rms}}\right). \tag{29}$$

We can now substitute Eq. 29 into Eq. 27, so that we obtain:

$$p_r = p_e exp\left(\frac{u0}{u_{rms}}\right) exp\left(\frac{-u}{u_{rms}}\right), \tag{30}$$

and when simplifying this equation we get

$$p_r = p_e exp\left(\frac{-u + u0}{u_{rms}}\right). \tag{31}$$

Since the true area of contact is linearly related to p_r [25], and the friction force is similarly related to the true area of contact, we find that the relationships for both can be obtained as:

$$A = A_0 exp(\frac{-u + u_0}{u_{rms}}), \tag{32}$$

and thus that

$$F_f = F_{f,0} exp(\frac{-u + u_0}{u_{rms}}). \tag{33}$$

Here, A_0 and $F_{f,0}$ are the initial true area of contact and initial friction force respectively, corresponding to the initial load force and u_0.

APPENDIX B
DETERMINING VIBRATION AMPLITUDE

Resonance frequencies: To find the range of the mechanical resonance frequencies of the Langevin transducers, we first performed a measurement with a RCL meter to determine the range of the electrical resonance frequencies. A sweep sine from 1 Hz to 100 kHz was sent to both of the transducers, which resulted a resonance frequency at $38.31 kHz$ for transducer 1 and $38.57 kHz$ for transducer 2. Different resonance frequencies can occur because the Langevin is not perfect, but also because of the self-milled horn, that are not exactly equal. As the electrical resonance for both actuators would be around 38 kHz, we then sent a frequency sweep sine signal of duration $T = 1s$, from $30 kHz$ - $50 kHz$ to also determine the mechanical resonance frequency. While sending the sweep sine, the velocity amplitude of the vibration of the top of the horn with a Laser Doppler Vibrometer (LDV)(Polytec, OFV505) a controller with displacement decoder (OFV5000 Polytec) at a sampling frequency of $200 kHz$ for $1s$. By performing an Fourier Transfer on this velocity signal, we could identify the resonance frequency of the Langevin transducers with cones by means of a Bodeplot (depicted in Fig. 15). This resulted in resonant frequencies of $38.31 kHz$ and $38.57 kHz$ for the top and bottom transducer respectively.

From velocity to position: It is expected that the highest vibration amplitude can be found at the highest voltage input as the force of the piezoelectric material is proportional to the voltage. The LDV measurement at these locations resulted in a voltage signal that corresponded to the velocity amplitude of the vibration. In this study, the sensitivity of the LDV was set at 200 $mm/s/V$. Therefore the signal was first multiplied by 200, and after this divided by $2\pi\omega$, to transform the velocity signal into a position signal. The result of this calculation is depicted in Fig. 15. From here the peaks of the sine wave correspond to the maximal vibration amplitude.

Vibration amplitude over voltage: Nonlinearities in Langevin transducers are not uncommon and seem to shift with voltage levels [26]. However, for this study it makes conceptually more sense to plot the measured values against a linear scale of vibration amplitudes, so we approximate a linear voltage-amplitude behavior. For simplicity we scaled our vibration amplitude between 0 and 3 μm for voltages between 0 and 150 V.
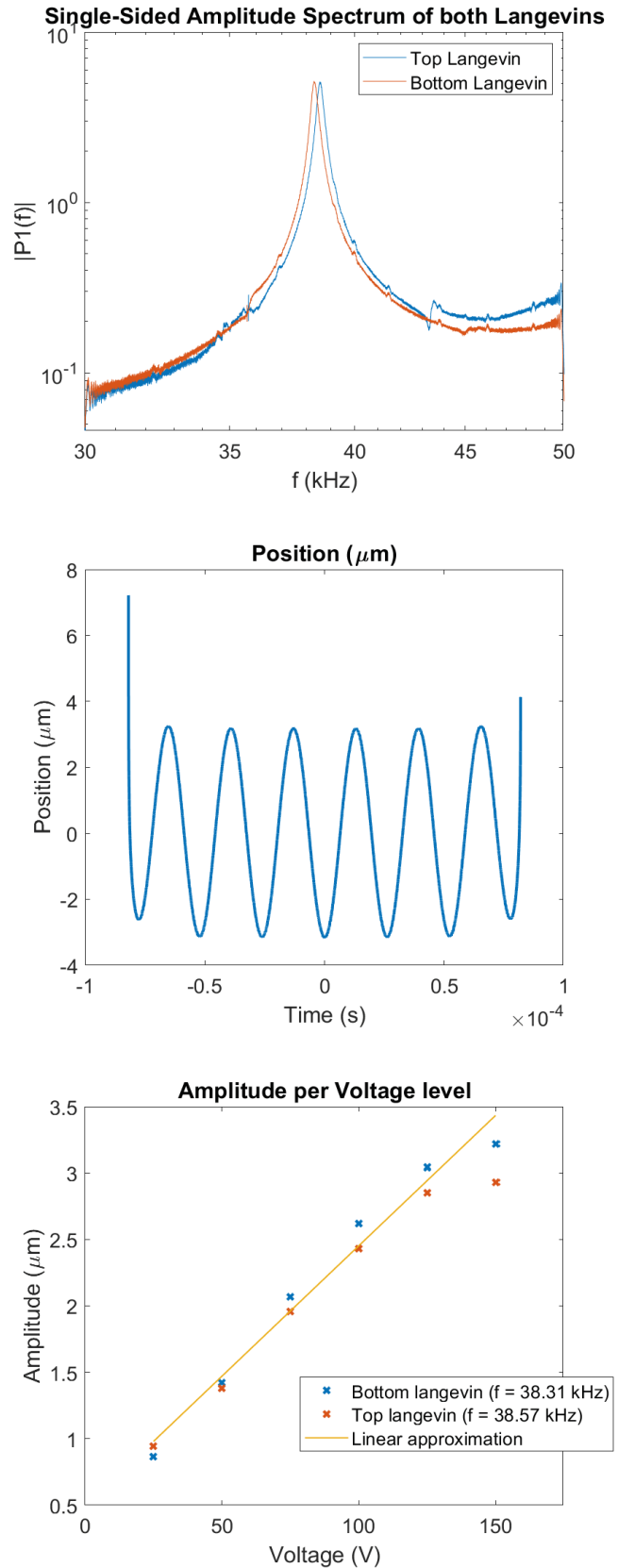
Fig. 15. Steps for identifying vibration amplitude of the Langevin transducers. First the bodeplot of both transducers was generated. Then a velocity signal was changed into a position signal. And lastly the peak amplitude was measured at different voltages.

APPENDIX C
MODEL

For our final model we used the following parameter values: $E = 3MPa$, $L_0 = 1.5mm$, $A = \pi * 0.01^2$, $q_0 = 2 * 10^4$, $v = 0.5$, and $p0 = 100kPa$. Here we depict the results of varying α, u_{rms}, and $F_{N,0}$ on Fn and Ff (note Fig. 16 and 18 are similar to the models depicted in Fig. 5, only enlarged).

Changing compression: Fig. 16 depicts the result of varying normal force and vibration amplitude on the measured normal force and friction force over vibration amplitude. We observe that for lower compression forces, a higher difference in initial friction and end friction can be achieved compared to for higher compression forces. At some point it is not possible anymore to obtain an increase in normal force.

(a) Vibrations 1 side   **(b)** Vibrations 2 sides
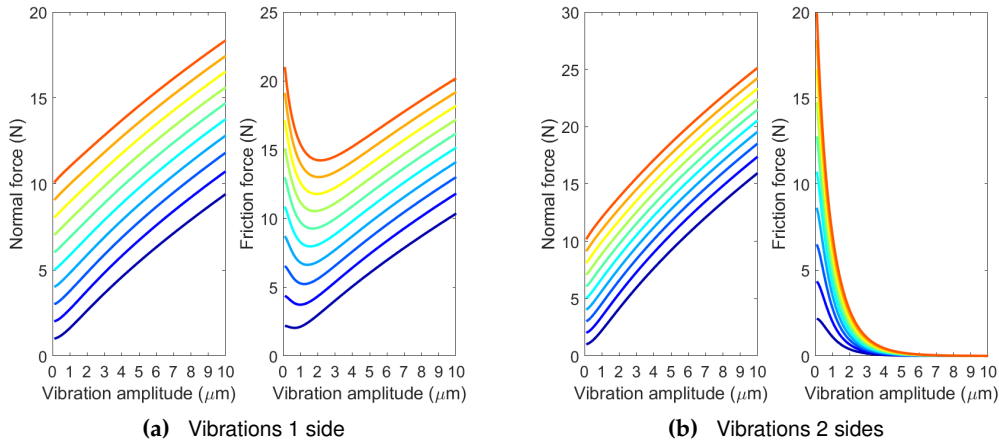
Fig. 16. Model for normal force and friction force for various initial compression values ($Fn_0 = 1N$ to $10N$) and changing vibration amplitude. Colors correspond to initial normal force, from lower values (blue) to higher values (red).

In our study we approximated most of the result by a first order regression curve. Here we show the the regression curves that followed from the model itself. We see that for most models actually a third order polynomial might be a better approximation. Nonetheless does a first order regression curve also captures the general trends quite well.

However, for our models we found these to be the best regression curves: For vibration from one sides a third order polynomial ($y = ax^3 + bx^2 + cx + d$) was chosen to fit best to the curves (see Fig. 17): for normal force we found coefficients $a = 0.0002, b = -0.0056, c = 0.0756, d = 0.2726$, and for the friction force $a = -0.0004, b = 0.0188, c = 0.1368, d = -0.2503$. For the vibrations from 2 sides, we found a third order polynomial best fitting to the normal force data ($a = 0.0039, b = -0.907, c = 0.5626, d = 14.4953$), and a first order polynomial ($y = ax + b$) for the friction force model ($a = -0.9997b = -0.0004$).

(a) Model regression vibrations 1 side   **(b)** Model regression vibrations 2 sides
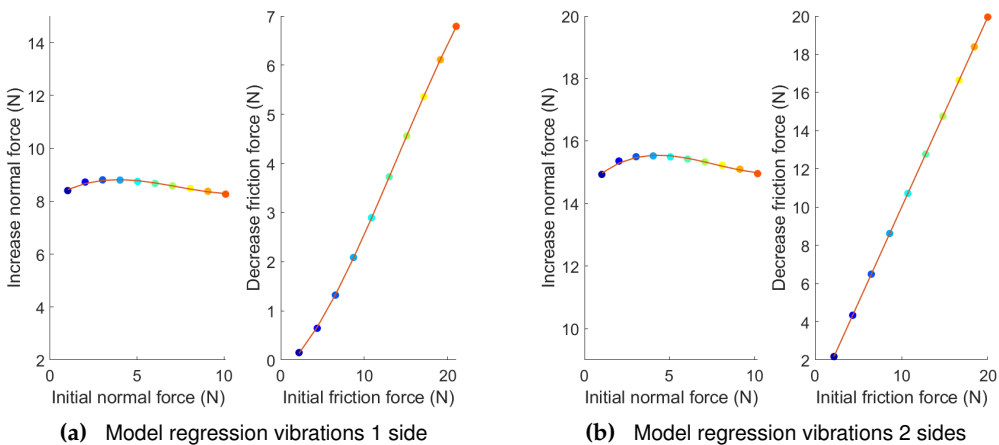
Fig. 17. Regression for models normal force and friction force for various initial compression values ($Fn_0 = 1N$ to $10N$) and changing vibration amplitude. Colors correspond to initial normal force, from lower values (blue) to higher values (red).

Changing roughness: Fig. 18 depicts the result of varying surface roughness and vibration amplitude on the measured normal force and friction force. We observe that for lower roughness values, thus smoother surfaces, a higher difference in initial friction and minimal friction can be achieved compared to for higher roughness values.

(a) Vibrations 1 side   **(b)** Vibrations 2 sides
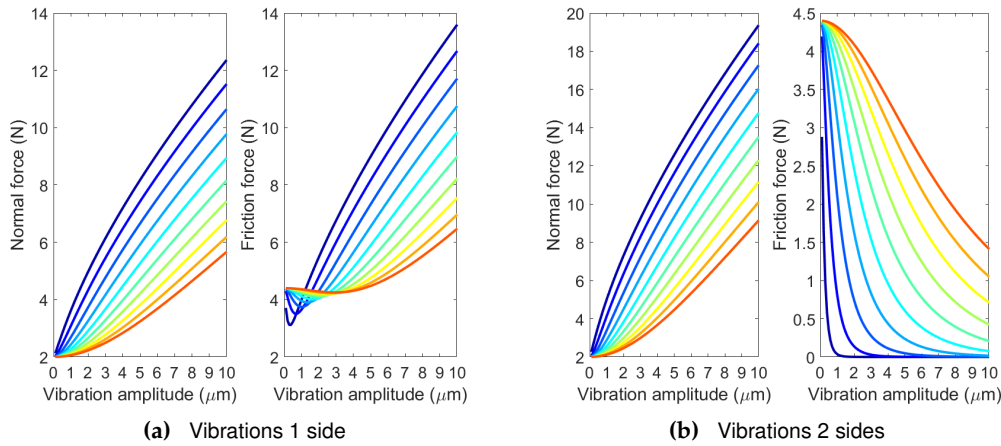
Fig. 18. Model for normal force and friction force for various roughness values ($u_{rms} = 1\mu m$ to $10\mu m$) and changing vibration amplitude. Colors correspond to initial normal force, from lower values (blue) to higher values (red).

Within our study we approximated the force increases and decreases by first order polynomials, but also here we see that actually third and fourth order polynomials approximate the regression curves better. For the change in roughness with vibrations from one side we see that for the normal force the regression can be described with a third order polynomial with coefficients $a = 0.0002, b = -0.008, c = -0.0160, d = 0.1120$ for the increase in normal force between $\alpha = 0\mu m$ and $\alpha = 10\mu m$. For the friction force we depicted the regression between the friction at $\alpha = 0$, and the minimal friction force, and found coefficients of $a = -0.0071, b = 0.1056, c = -0.5750, d = 1.2733$. The normal force from 2 sides increased between $\alpha = 0\mu m$ and $\alpha = 10\mu m$ with coefficients $a = 0.0006, b = -0.0045, c = -0.0134, d = 0.1815$. Lastly for the friction from two sides we studied the gradient between friction values of 1.5 N and 2.5 N, because here the curves show a similar behavior. We found that the gradient could best be described with a fourth order polynomial ($y = ax^4 + bx^3 + cx^2 + dx + e$) with coefficients $a = 0.0030, b = -0.0515, c = 0.3505, d = 2.0339, e = -1.5360$.

(a) Model regression vibrations 1 side   **(b)** Model regression vibrations 2 sides
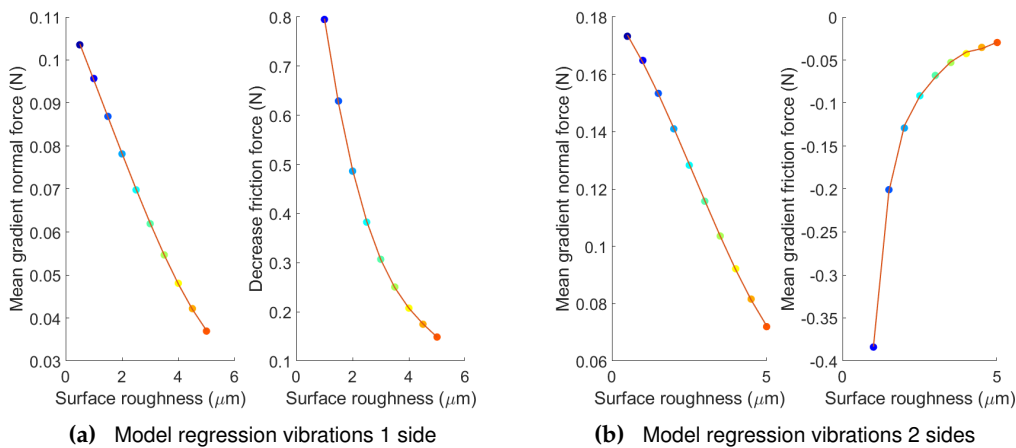
Fig. 19. Regression for models normal force and friction force for various initial compression values ($Fn_0 = 1N$ to $10N$) and changing vibration amplitude. Colors correspond to initial normal force, from lower values (blue) to higher values (red).

APPENDIX D
RAW DATA

During each repetition the normal force was measured for a time period of 21 seconds (see Fig. 20), while the rubber plate was being pulled from between the vibrating surface(s). In each trial the first 10 seconds were needed to saturate. For the calculation of the mean of each trial, we analysed the last 10 seconds only (indicated with grey area). This corresponds to the last 1 cm on the position stage.
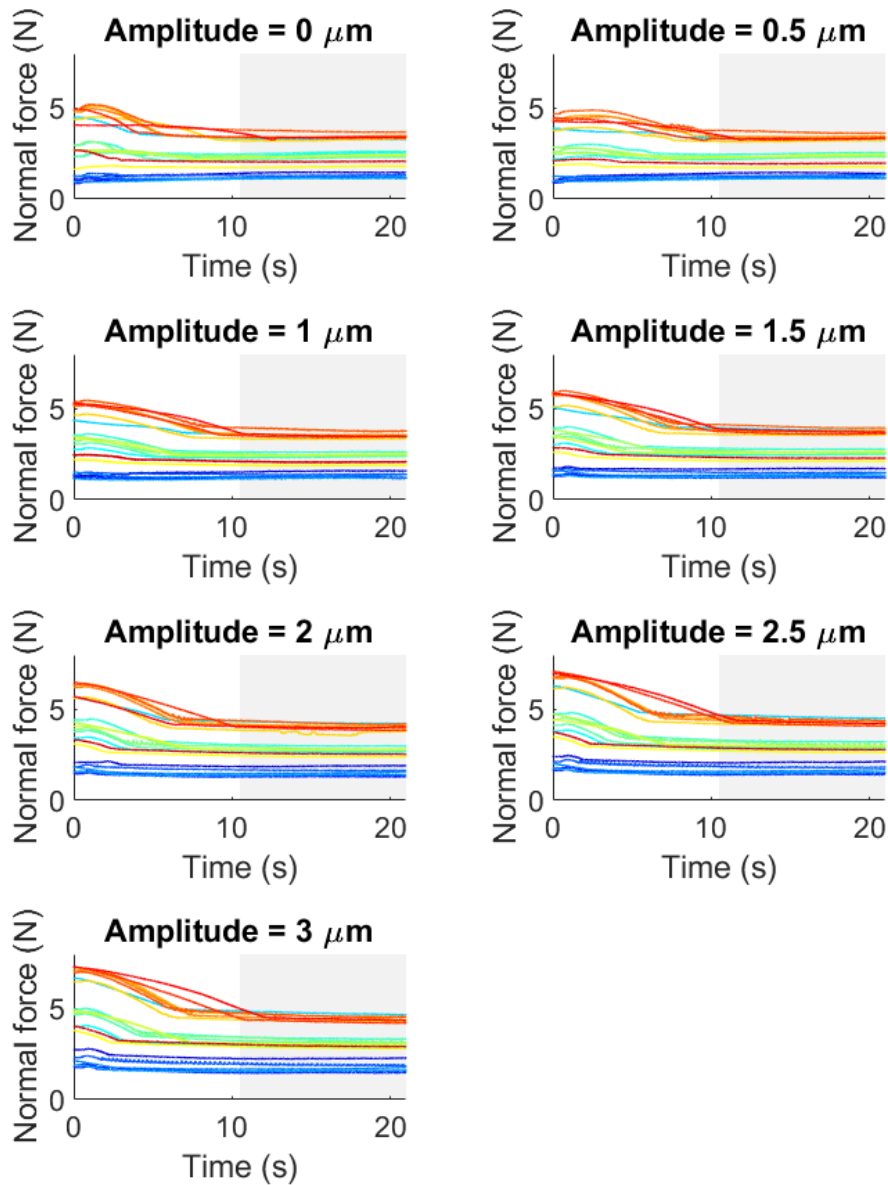
Fig. 20.   Raw **normal force** over time corresponding to 8a, 21 repetitions of each experiment for varying **initial compression**. Normal force saturates after approximately 10 seconds, this part is taken for the analysis of the mean normal force for that repetition (indicated with grey shaded area). Different subplots correspond to different vibration amplitude values. Colors correspond to chronology of measurement (blue as first, to red as end).
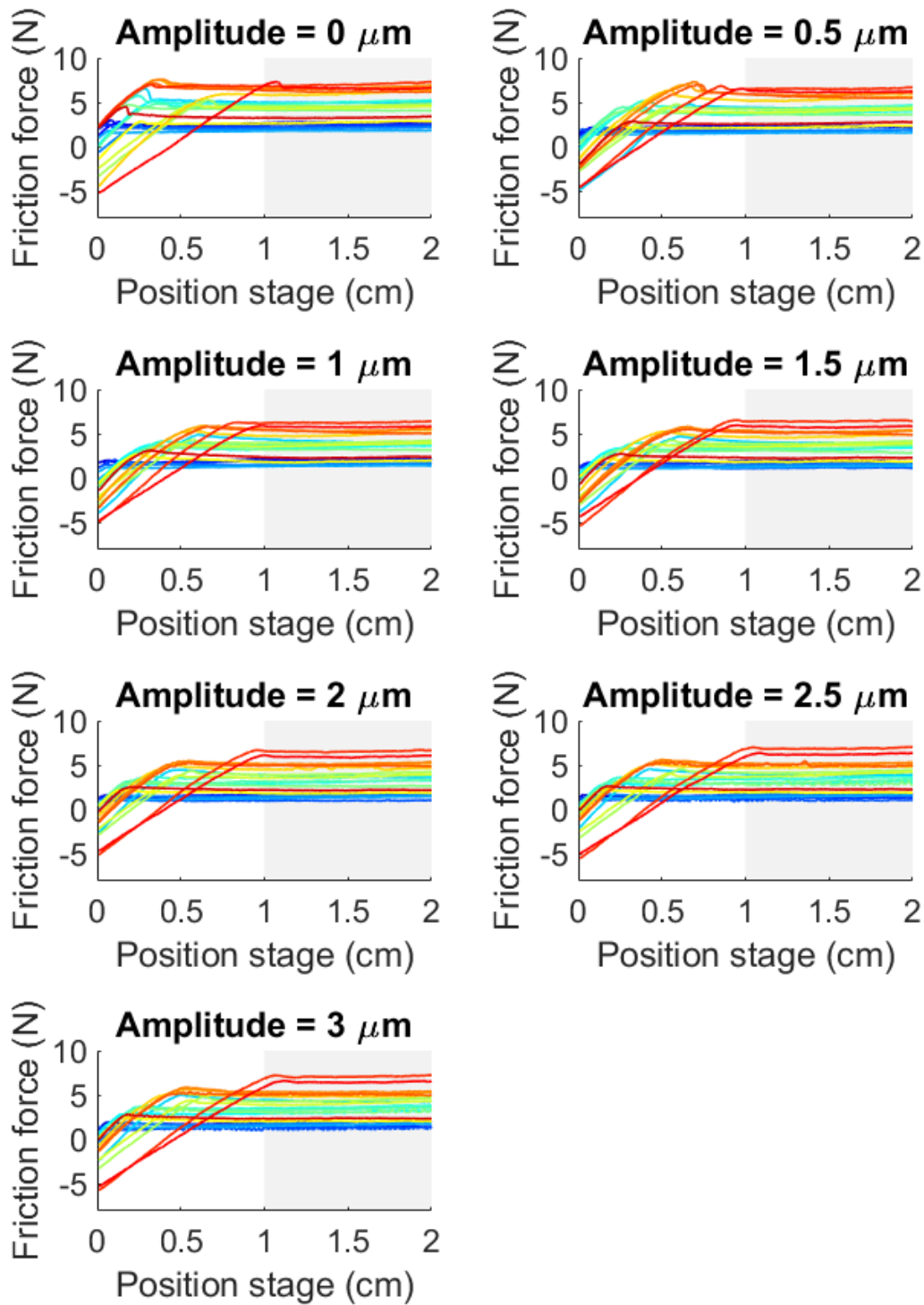
Fig. 21. Raw **friction force** over time corresponding to 8b, 21 repetitions of each experiment for varying **initial compression**. Friction force saturates after approximately 1 cm, this part is taken for the analysis of the mean friction force for that repetition (indicated with grey shaded area). Different subplots correspond to different vibration amplitude values. Colors correspond to chronology of measurement (blue as first, to red as end).
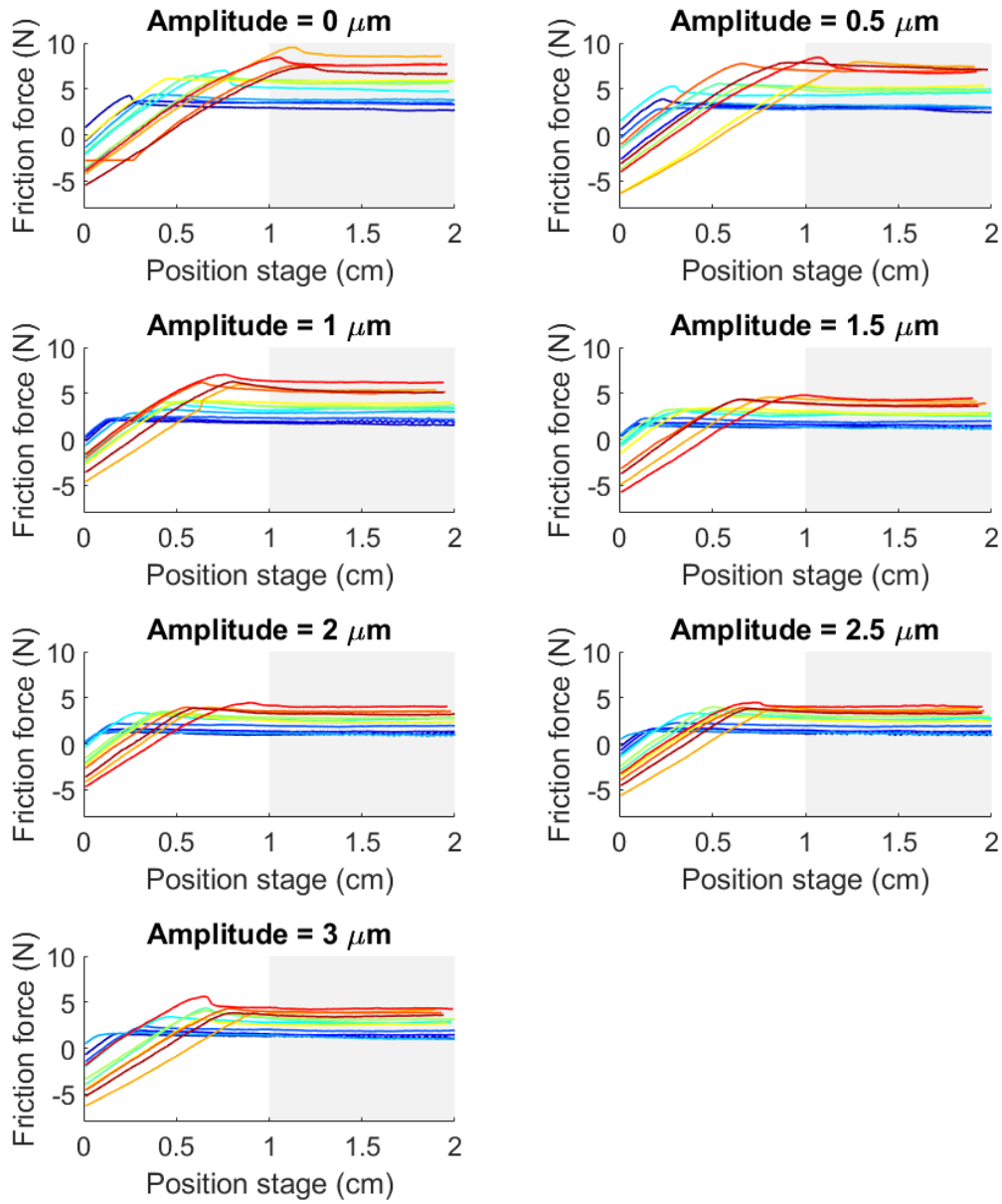
Fig. 22. Raw **friction force** over time corresponding to 9, 18 repetitions of each experiment for varying initial **initial compression**. Friction force saturates after approximately 1 cm, this part is taken for the analysis of the mean friction force for that repetition (indicated with grey shaded area). Different subplots correspond to different vibration amplitude values. Colors correspond to chronology of measurement (blue as first, to red as end).
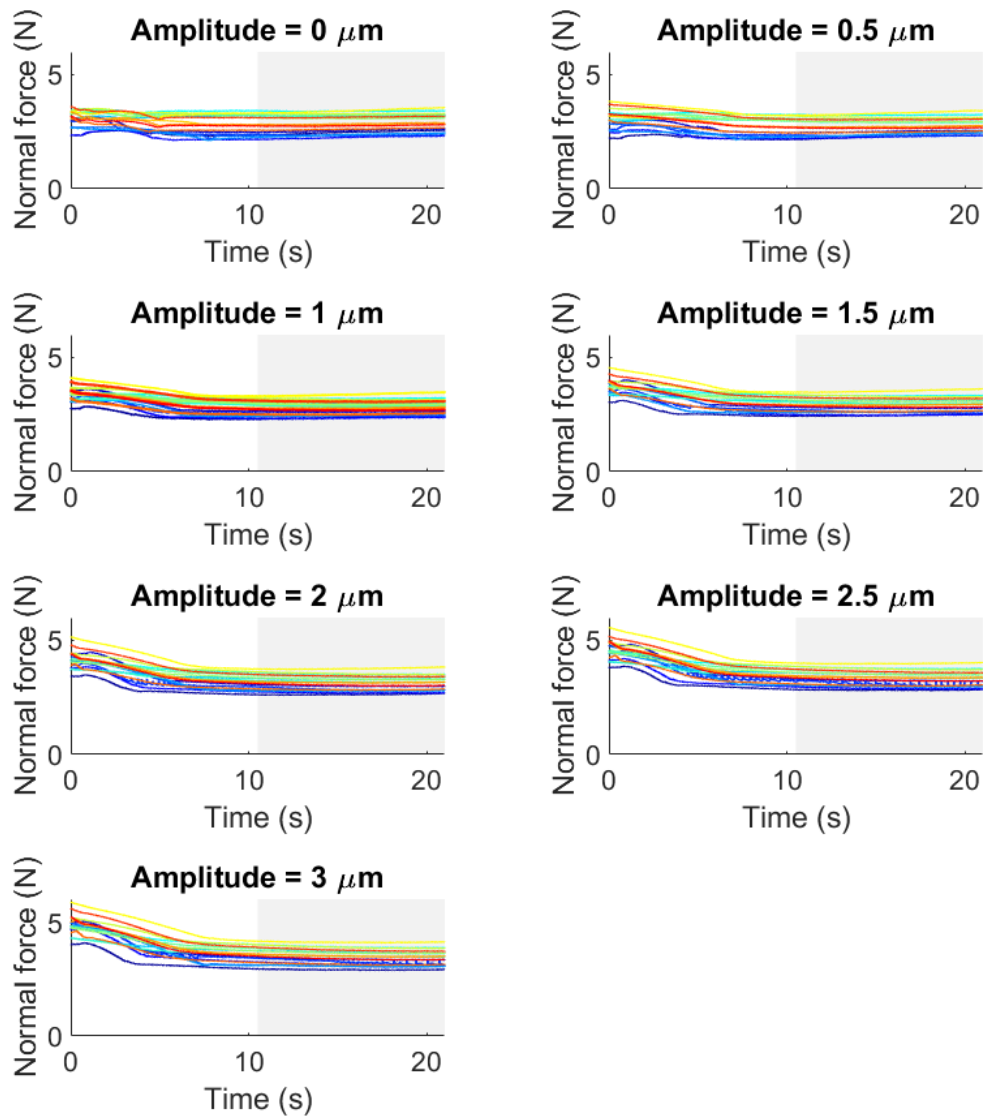
Fig. 23. Raw **normal force** over time corresponding to Fig. 10a, 18 repetitions of each experiment for varying **surface roughness**. Normal force saturates after approximately 10 seconds, this part is taken for the analysis of the mean normal force for that repetition (indicated with grey shaded area). Different subplots correspond to different vibration amplitude values. Colors correspond to chronology of measurement (blue as first, to red as end).
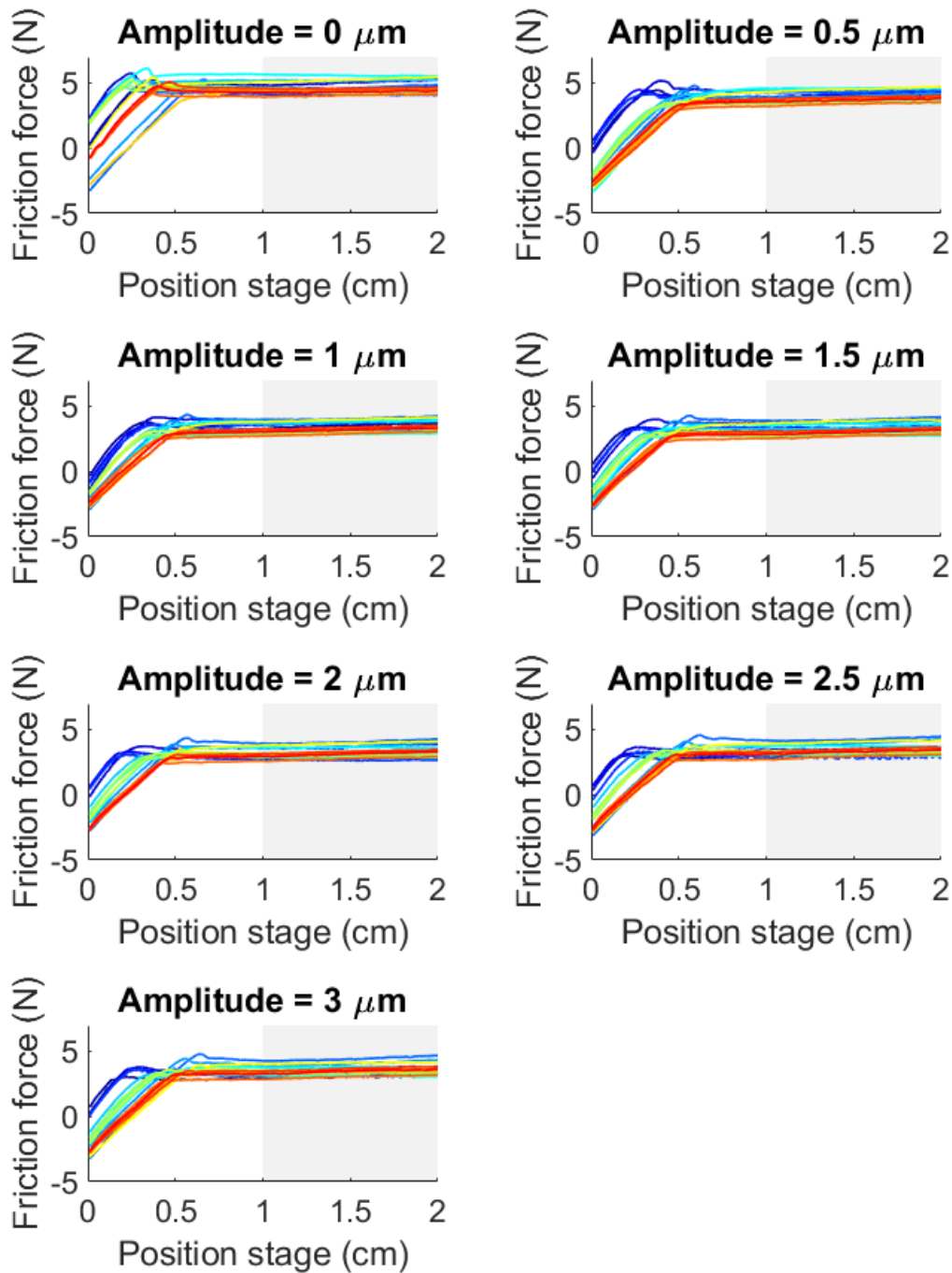
Fig. 24. Raw **friction force** over time corresponding to Fig. 10b, 18 repetitions of each experiment for varying **surface roughness**. Friction force saturates after approximately 1 cm, this part is taken for the analysis of the mean friction force for that repetition (indicated with grey shaded area). Different subplots correspond to different vibration amplitude values. Colors correspond to chronology of measurement (blue as first, to red as end).
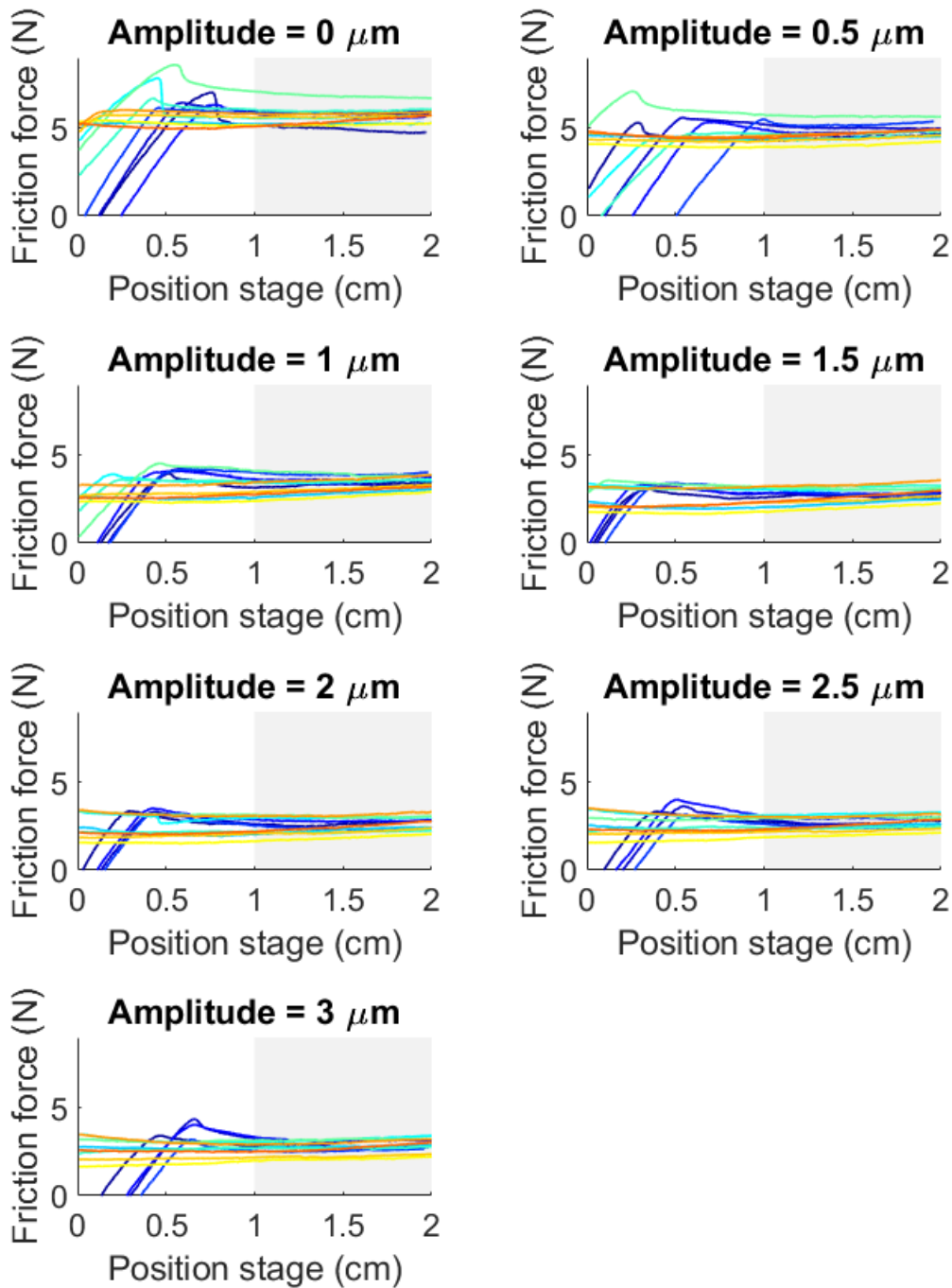
Fig. 25. Raw **friction force** over time corresponding to Fig. 11, 12 repetitions of each experiment for varying initial **surface roughness**. Friction force saturates after approximately 1 cm, this part is taken for the analysis of the mean friction force for that repetition (indicated with grey shaded area). Different subplots correspond to different vibration amplitude values. Colors correspond to chronology of measurement (blue as first, to red as end).

APPENDIX E
ROUGHNESS MEASUREMENTS

The model used in this study is highly dependent on the surface roughness of the material in play. In this study we obtained three different surface roughness samples, by sandpapering the rubber material we used with different grain sizes. To obtain an equally distributed surface roughness, we taped the sandpaper to the table , and the rubber to a fully flat surface (see Fig. 26). Then, we we moved the metal plate with the rubber over the sandpaper in a circular motion for 30 times. Afterwards, we performed a surface roughness measurement at the optics lab at the Precision and Micro-systems department of the TU Delft to identify how the roughness had changes. The measurement is visualized in Fig. 27 - 29.
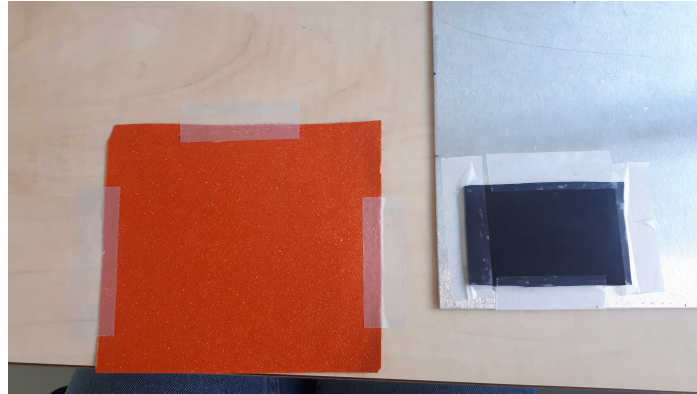
Fig. 26. Left: sandpaper taped to the table. On the right: rubber sample taped to steel plate.

Roughness plate 1: The first plate was just the rubber in its original state, without being sandpapered. A surface roughness measurement revealed a surface roughness (u_{rms}) of approximately 1.5 μm. This makes this sample the smoothest of all three.
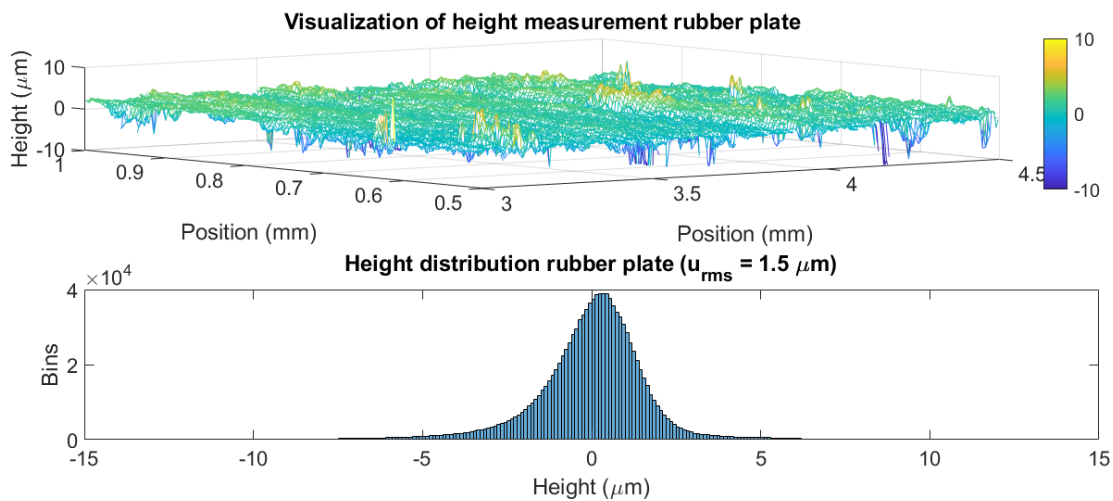
Fig. 27. Visualization of height distribution rubber of plate 1.

Roughness plate 2: The second plate was sandpapered with a sandpaper 150 grit. A surface roughness measurement revealed a surface roughness (u_{rms}) of approximately 4.4 μm. This makes this sample the second smoothest.
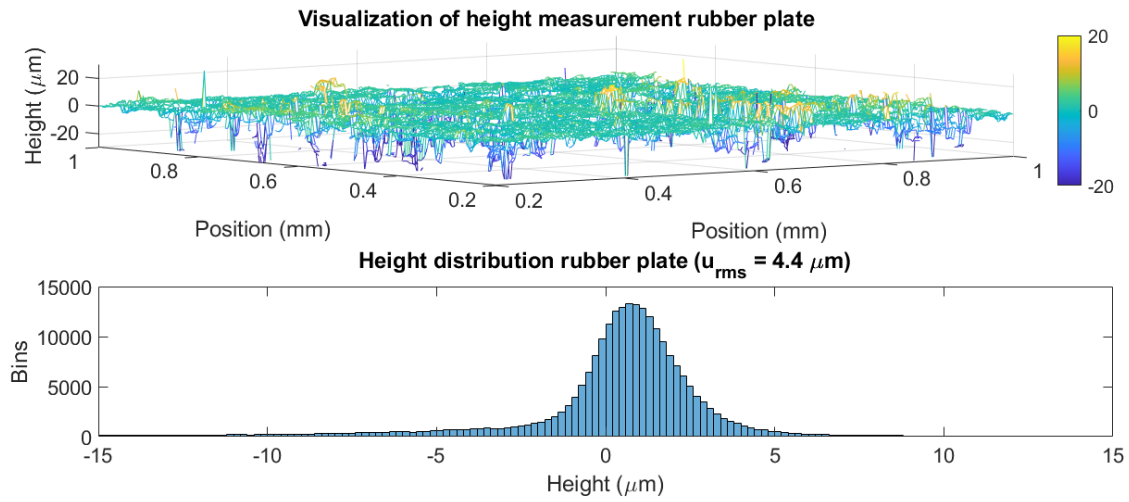
Fig. 28.   Visualization of height distribution rubber of plate 2.

Roughness plate 3: The third plate was sandpapered with a sandpaper 80 grit. A surface roughness measurement revealed a surface roughness (u_{rms}) of approximately 8.2 μm. This makes this sample the roughest one.
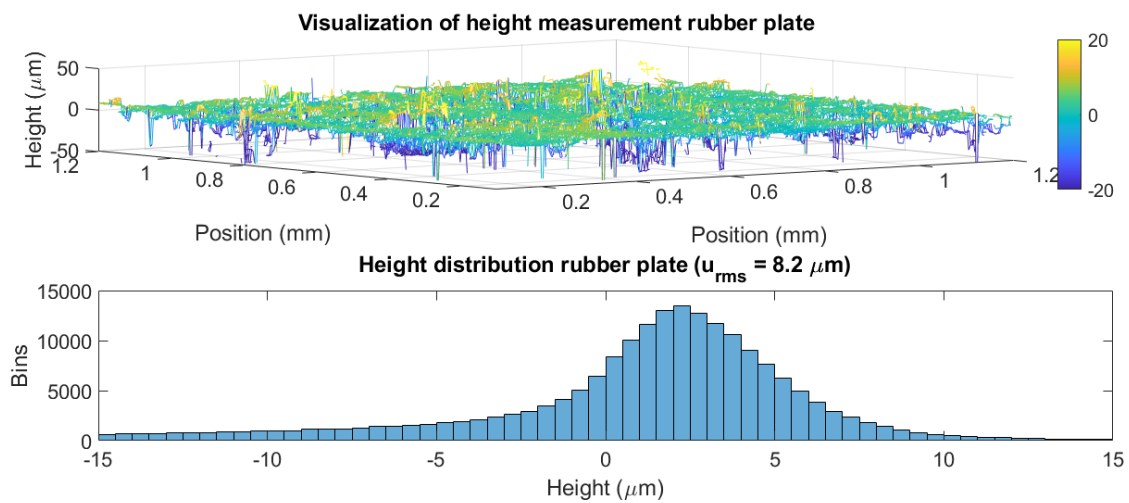
Fig. 29.   Visualization of height distribution rubber of plate 3.

APPENDIX F
UNCERTAINTY ANALYSIS

The measurements of the normal force we found that it was difficult to keep the initial normal force constant, and that there always appeared to be some variation in the force data between measurement. The variation in the initial normal force data at zero amplitude might be contributed to two things: the limitation in precision of manually adjusting the linear stage, and drift of the normal force sensor.

Inaccuracy manual stage: The manual stage can make discrete steps of 10 micrometer (XR25C, Thorlabs). We estimate that with the naked eye an accuracy of $10 + / - 1 \mu m$ can be achieved. We performed an experiment to check the effect of this manual error on the normal force to be measured. For this, we measured the normal force at 5 different compression rates, and repeated this for 5 times. The results are depicted in Fig. 30. We assumed that the relationship between the indentation depth and the normal force measured, should be linear, as the force arises from the rubber layer being compressed, which, at these indentation depths, should result in a linear force. The error from the manual stage is probably around $1.25 * 0.1 = 0.125N$. Note that once the manual stage is set at a certain distance, it's more of a bias than an error, as it will be the same for all other measurements following from this setting.
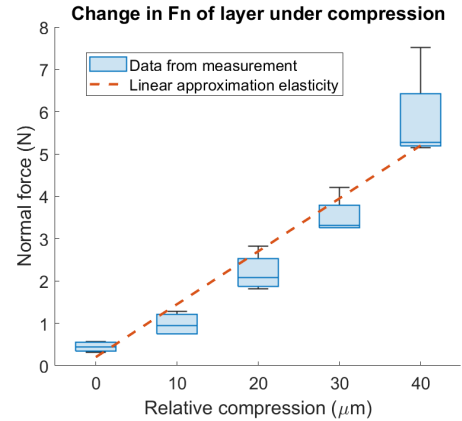
Fig. 30. Change in Fn under compression. The measurements were repeated five times and a linear trendline was fitted to the data. The gradient of the linear line is $1.25N$ per $10 \mu m$.

Drift normal force sensor: We found some variety in the normal force sensor data after the experiments had been performed, and tried to quantify this amount. Also we were wondering whether turning the vibrations on and off would have an effect on the normal force data. We performed the following experiments to get a feeling for the sensor variety: First we would calibrate the force sensor and move the stage to a distance at which we would measure a normal force of approximately $3N$. This would be the first measurement at $t = 0s$, which is also visualized in Fig. 31. Secondly, we would actuate the Langevin transducer at 25V (corresponding to 0.5 vibration amplitude) for 20 seconds, then turn of the actuation, so no vibrations would be applied, and after approximately 5 seconds again measure the normal force. This would be the second measurement at $t = 30sec$ (second measurement in Fig. 31). We would repeat this process 7 times, for each of the actuation levels that were also used in the real experiment, in the same order as in the real experiment, which results in one of the plots of Fig. 31. For extra certainty, we repeated this experiment 3 times, as can also be seen in the figure.
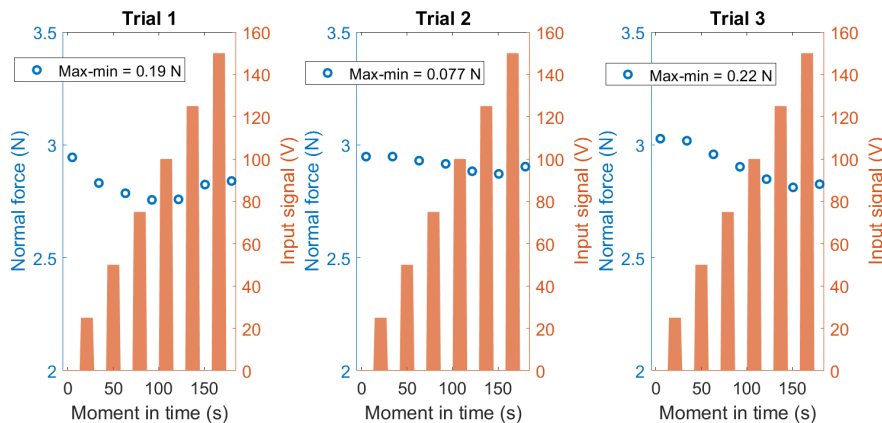
Fig. 31. Output normal force sensor data: The plot shows the raw data obtained from the normal force data for three different trials, with in every trial 7 measurement points (at $t = 0s$, $t = 30s$, $t = 60s$, $t = 90s$, $t = 120s$, $t = 150s$, and $t = 180s$)). Between each measurement, the transducer was excited with the same voltage levels as in the experiment, in the same order, so first with 25V, then 50V, etc. Each normal force measurement took $3s$ to perform. All measurements show quite a constant line, so that the mean normal force at each data point can be obtained by averaging over time.

What we would expect to see in a robust sensor, is the exact same measurement regardless of what amount of excitation level had been applied in the mean time. However, we can observe in Fig. 31 that actually the values changed slightly over time. Nonetheless, there does not seem to be an clear relationship to the applied voltage and the effect on the next normal force measurement, it's rather random. Therefore it might be that there is just a drift in the normal force sensor already, regardless of any voltage being applied. To check this, we performed a second experiment in which we would no apply any voltage to the transducer in between measurements, but perform 7 measurements in a row, each time with approximately 30 seconds in between. The results of this experiments are depicted in Fig. 32.
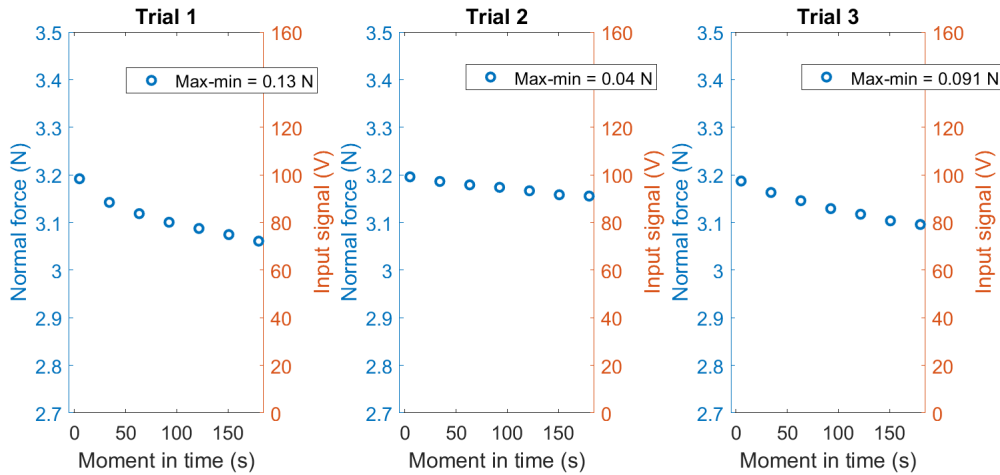
Fig. 32. Output normal force sensor data: The plot shows the raw data obtained from the normal force data for three different trials, with in every trial 7 measurement points (at $t = 0s$, $t = 30s$, $t = 60s$, $t = 90s$, $t = 120s$, $t = 150s$, and $t = 180s$)). Between measurements the transducers were not excited. Each normal force measurement took $3s$ to perform. All measurements show quite a constant line, so that the mean normal force at each data point can be obtained by averaging over time.

From this second experiment we see that there seems to be a drift in the normal force sensor over time, but that over a period of $180s$, it only decreases, not increases. As we do see an increase in force as well at some point when we apply a vibration in the between measurements, we assume that both the drift of the sensor, as well actuating the Langevin transducer have an effect on the normal force.

An explanation for this variety in force due to actuation of the transducers can be linked to what we discussed before: the effect of the inaccuracy of the linear stage. It might be that applying vibrations slightly changes the relative orientation of parts in the setup, and as we assumed that a change of about $1\mu m$ can cause a force difference of $0.125N$, this could be a feasible explanation for the variety in normal force.

Nonetheless, as the variation is small and rather random when the transducers are actuated in between, we just assume it to be measurement noise and neglect the effects during analysis.